RESEARCH ARTICLE

NANO · MICRO small
www.small-journal.com

Collagen Signaling via DDR1 Exacerbates Barriers to Macromolecular Drug Delivery in a 3D Model of Pancreatic Cancer Fibrosis

Mayu Ohira, Moe Kitamura, Hiroyo Iwasaki, Haruko Ohta-Okano, Hiyori Tsujii, Reika Nakamura, Takuya Nakazawa, Akihiro Nishiguchi, Masaya Yamamoto, Kensuke Osada, Shinichi Toyooka, Horacio Cabral, Atsushi Masamune, Mitsunobu R. Kano, and Hiroyoshi Y. Tanaka**

Fibrosis is a significant barrier to drug delivery in pancreatic ductal adenocarcinoma (PDAC) and contributes to its dismal prognosis. Pancreatic stellate cells (PSCs) drive fibrosis by excessively secreting extracellular matrix proteins such as collagen I. Collagen I is thought to physically obstruct the delivery of macromolecules, such as albumin, antibodies, and nanomedicines. Apart from its structural role, collagen signals through dedicated cell surface receptors, such as the discoidin domain receptors (DDR) 1/2. However, whether and how collagen signaling contributes to fibrotic barrier generation remains uncharacterized. Here, a 3D culture model of PDAC fibrosis constructed from patient PSCs is used to assess the contribution of DDR1/2-mediated collagen signaling. DDR1/2 inhibition diminishes collagen I expression in PSCs to enhance macromolecular delivery. Moreover, MEK inhibitors exacerbate the fibrotic barrier by up-regulating collagen I, an effect reversed by inhibiting DDR1/2. Through isoform-specific targeting, inhibiting DDR1, but not DDR2, is shown to be effective. Downstream of DDR, the involvement of the PI3K/AKT/mTOR pathway is demonstrated, particularly alternative mTOR complexes involving MEAK7 and GIT1. Altogether, the results show in vitro that DDR1-mediated collagen signaling exacerbates the fibrotic barrier and may be targeted to enhance macromolecular drug delivery in PDAC.

1. Introduction

Pancreatic cancer, ≈95% of which are pancreatic ductal adenocarcinomas (PDAC), is characterized by prominent stromal fibrosis occupying 40–80% of tumor tissue.[1] Fibrosis poses a significant physical barrier to drug delivery, and is particularly problematic for the delivery of macromolecules, such as albumin, therapeutic antibodies, and nanomedicines.[2,3] Indeed, an intravenously administered drug must pass through this fibrotic tissue with a median thickness of 10–30 µm to reach tumor cells.[4,5] Fibrosis thus contributes to the dismal prognosis of PDAC, with a 5-year survival rate just above 10%.[6,7] Targeting of fibrosis therefore is necessary to enhance the delivery and efficacy of therapeutics and improve treatment outcome in PDAC. Though the failure of stromal ablation strategies points at the need for precise targeting of fibrotic processes,[3,8] our understanding of the molecular mechanisms driving fibrotic barrier generation remains limited.

M. Ohira, M. Kitamura, H. Iwasaki, H. Ohta-Okano, H. Tsujii, R. Nakamura, H. Y. Tanaka
Department of Pharmaceutical Biomedicine
Graduate School of Medicine
Dentistry and Pharmaceutical Sciences
Okayama University
1-1-1 Tsushima-naka, Kita-Ku, Okayama-Shi, Okayama 700-8530, Japan
E-mail: hiroyoshi.y.tanaka@okayama-u.ac.jp

The ORCID identification number(s) for the author(s) of this article can be found under https://doi.org/10.1002/smll.202506926

DOI: 10.1002/smll.202506926

T. Nakazawa, M. R. Kano
Department of Pharmaceutical Biomedicine
Graduate School of Interdisciplinary Science and Engineering in Health Systems
Okayama University
1-1-1 Tsushima-naka, Kita-Ku, Okayama-Shi, Okayama 700-8530, Japan
E-mail: mitkano@okayama-u.ac.jp

A. Nishiguchi
Biomaterials Field
Research Center for Macromolecules and Biomaterials
National Institute for Materials Science
1-1 Namiki, Tsukuba-Shi, Ibaraki 305-0044, Japan

M. Yamamoto
Department of Materials Processing
Graduate School of Engineering
Tohoku University
6-6-02, Aza-Aoba Aramaki, Aoba-Ku, Sendai-Shi, Miyagi 980-8579, Japan

Resident fibroblastic cells of the pancreas, pancreatic stellate cells (PSC), orchestrate the fibrotic process. PSCs are mainly responsible for the excessive production of extracellular matrix (ECM).[9,10] Collagen I is the most abundant ECM component in PDAC,[11] and its excessive deposition is believed to physically obstruct macromolecular delivery.[2,3,12] Apart from its role as a structural protein, collagen I also signals through transmembrane receptors to regulate various cellular processes.[13,14] However, the involvement of collagen I signaling in fibrotic barrier generation remains uncharacterized. Interestingly, the collagen-activated receptor tyrosine kinase discoidin domain receptors (DDR) 1/2 seem to be involved in fibro-inflammatory processes in the pancreas. Elevated expressions of both DDRs were reported in the cerulein-induced acute pancreatitis model, and ECM deposition was ameliorated by imatinib, which has inhibitory activity against DDR1/2.[15] We thus hypothesized that targeting collagen I signaling through DDRs may be effective in overcoming the fibrotic barriers to macromolecular drug delivery in PDAC.

Here, we leverage a 3D cell culture model of the fibrotic tissue in PDAC (3D-PDAC fibrotic tissues[4,16]) constructed from patient-derived PSCs to assess the role of DDR1/2-mediated collagen signaling in fibrotic barrier generation. We demonstrate that pharmacological targeting of DDR1/2 diminishes collagen I expression in PSCs and enhances permeability of 3D-PDAC fibrotic tissues to macromolecules, including clinically relevant nanomedicines. Interestingly, we show that MEK inhibitors, which previously failed to demonstrate clinical efficacy despite signaling overactivation due to *KRAS* mutations prevalent in PDAC,[17,18] up-regulate collagen I expression in PSCs. MEK inhibitors exacerbated the fibrotic barrier at clinically relevant doses, an effect that could be reversed by DDR1/2 inhibition. Notably, using isoform-specific inhibitors and siRNAs, we establish that targeting of DDR1, but not DDR2, enhances macromolecular permeability. Downstream of DDRs, we demonstrate the involvement of the phosphatidylinositol 3-kinase (PI3K)/AKT/mammalian target of rapamycin (mTOR) pathway. The regulation of collagen I expression in PSCs and macromolecular permeability of 3D-PDAC fibrotic tissues did not require the canonical mTOR complexes (mTORC), mTORC1 or mTORC2. In contrast, the combined targeting of alternative mTORC components MEAK7 and GIT1 diminished collagen I expression and enhanced macromolecular permeability. Altogether, we demonstrate that DDR1-mediated collagen I signaling exacerbates the fibrotic barrier and may be targeted to enhance macromolecular drug delivery in PDAC.

M. Yamamoto
Division of Biomedical Engineering for Diagnosis and Treatment
Graduate School of Biomedical Engineering
Tohoku University
6-6-02, Aza-Aoba Aramaki, Aoba-Ku, Sendai-Shi, Miyagi 980-8579, Japan
K. Osada
Department of Molecular Imaging and Theranostics
Institute for Quantum Medical Science
National Institutes for Quantum Sciences and Technology (QST)
4-9-1 Anagawa, Inage-Ku, Chiba-Shi, Chiba 263-8555, Japan
S. Toyooka
Department of General Thoracic Surgery and Breast and Endocrinological Surgery
Graduate School of Medicine
Dentistry and Pharmaceutical Sciences
Okayama University
2-5-1 Shikata-cho, Kita-Ku, Okayama-Shi, Okayama 700-8558, Japan
H. Cabral
Department of Bioengineering
Graduate School of Engineering
The University of Tokyo
7-3-1 Hongo, Bunkyo-Ku, Tokyo 113-8656, Japan
A. Masamune
Division of Gastroenterology
Graduate School of Medicine
Tohoku University
1-1 Seiryo-machi, Aoba-Ku, Sendai-Shi, Miyagi 980-8574, Japan

2. Results

2.1. Pharmacological Inhibition of DDR1/2 Attenuates Collagen I Expression by PSCs to Enhance Macromolecular Permeability of 3D-PDAC Fibrotic Tissues

To assess the role of collagen signaling through DDR1/2 in fibrotic barrier generation, we first utilized VU-6015929, a DDR1/2 inhibitor with comparable activity against both isoforms.[19] VU-6015929 decreased collagen I expression by PSCs cultured in 2D (**Figure 1A–C**) and collagen I deposition in 3D-PDAC fibrotic tissues (Figure 1D–F). While VU-6015929 diminished growth of PSCs cultured in 2D on conventional plastic culture-ware (Figure S1A–D, Supporting Information), VU-6015929 at the concentrations tested did not affect the thickness of 3D PDAC-fibrotic tissues (Figure 1G–J). This is in line with our previous report reporting relatively higher viability of PSCs in 3D PDAC-fibrotic tissues against inhibitor treatment compared to 2D culture,[16] and likely results from altered microenvironmental cues due to the 3D experimental setup.[20]

Next, to investigate the effect of DDR1/2 inhibition on macromolecular permeability, we loaded fluorescein isothiocyanate (FITC)-labeled dextrans with an average molecular weight of 2000 kDa to the 3D-PDAC fibrotic tissues. Consistent with its effects on collagen I expression, 10 μM VU-6015929 enhanced permeation of 2000 kDa FITC-dextrans through the tissues (Figure 1K,L). Additional time course experiments revealed that permeability enhancement occurs between 24–48 h after initiation of VU-6015929 treatment (Figure S2A–C, Supporting Information). Together with the lack of effect of VU-6015929 on 3D-PDAC fibrotic tissue thickness, these results overall suggest that DDR1/2 inhibition enhances macromolecular permeability via a mechanism different from stromal ablation.

To ascertain if the observed enhancement in permeability of 3D-PDAC fibrotic tissues is dependent on macromolecular size, the permeation of smaller FITC-dextrans (150 or 70 kDa), as well as FITC-IgG antibodies and FITC-albumin were assessed (Figure S3A–H, Supporting Information). VU-6015929 at 10 μM enhanced permeation in both PSCs for all macromolecules tested except in the case of FITC-albumin, in which enhancement was seen in PSC #1 but not PSC #2 (Figure S3G,H, Supporting Information). This is perhaps due to the smaller size of albumin compared to

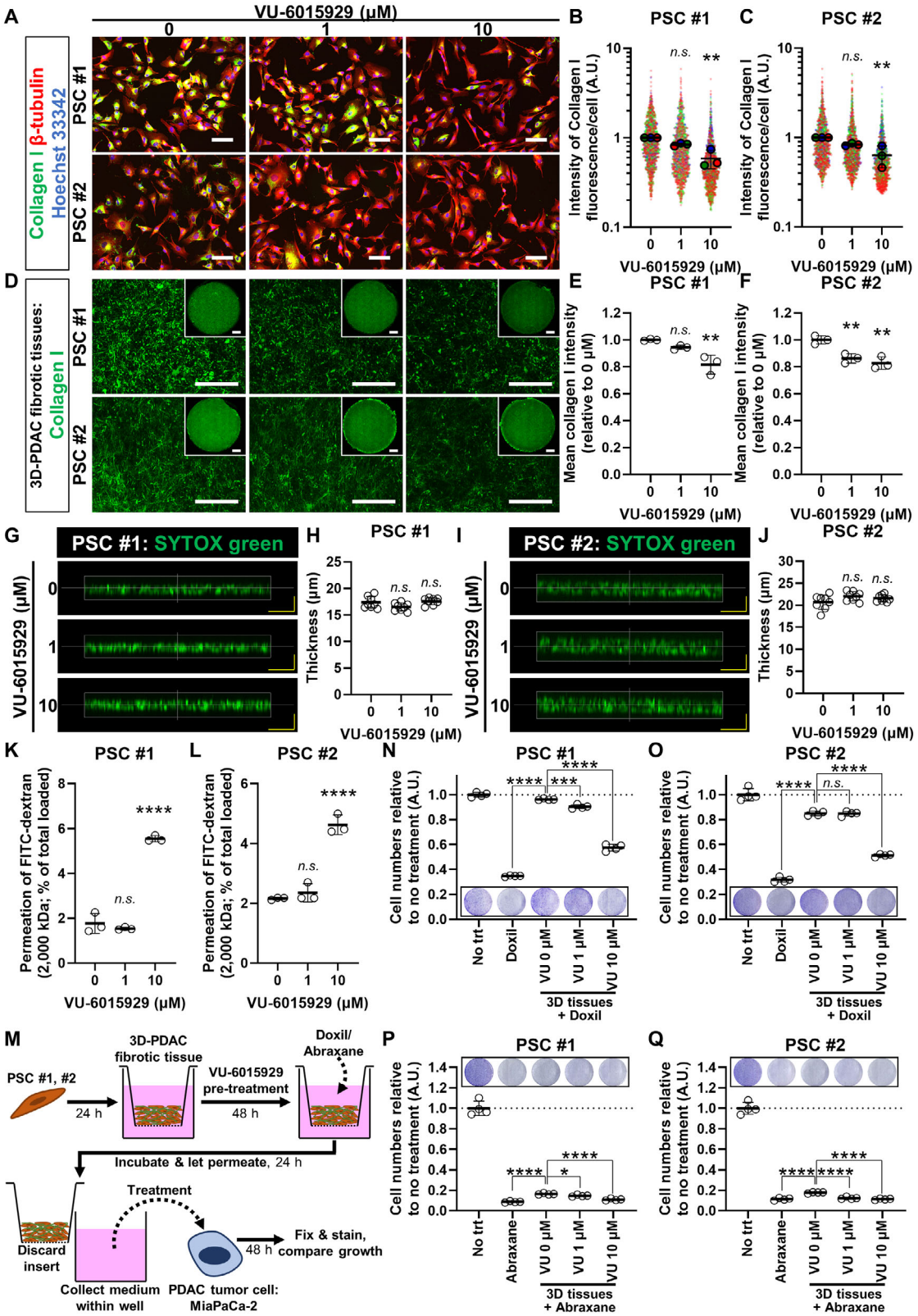

the others tested, showing the highest permeation even at baseline.

To test whether the observed enhancement in macromolecular permeability is sufficient to induce therapeutic effect, 3D-PDAC fibrotic tissues were pre-treated with VU-6015929 before administration of two clinical nanomedicine formulations, Doxil (liposomal doxorubicin) and Abraxane (*nab*-paclitaxel). Of note, Doxil and Abraxane were both used at 10 μg mL^{-1}, which is below the reported C_{max} values in patients.[21,22] Doxil and Abraxane used at this concentration suppressed PSC growth by up to ≈50% (Figure S4A–H, Supporting Information), but did not significantly diminish 3D-PDAC fibrotic tissue thickness (Figure S4I–L, Supporting Information). The media beneath the culture inserts containing the permeated nanomedicines were then collected and used to treat the PDAC cell-line MiaPaCa-2 to compare effect on cell growth (Figure 1M). Compared to direct administration of Doxil (Figure 1N,O) and Abraxane (Figure 1P,Q), the interposition of 3D-PDAC fibrotic tissues attenuated therapeutic effect. The diminution of therapeutic effect by 3D-PDAC fibrotic tissues was more pronounced for Doxil than Abraxane. While this seems counterintuitive given the greater nominal size of Abraxane (≈130 nm diameter) versus Doxil (≈100 nm),[23] the greater therapeutic effect of Abraxane may reflect its propensity to rapidly dissociate into smaller albumin-bound paclitaxel complexes.[23] Importantly, pre-treatment of 3D-PDAC fibrotic tissues with VU-6015929 led to a stronger suppression of MiaPaCa-2 cell growth (Figure 1N–Q). These results altogether suggest that VU-6015929 enhances macromolecular drug delivery through 3D-PDAC fibrotic tissues to improve therapeutic effect of clinical nanomedicines.

2.2. MEK Inhibitors Induce Collagen I Expression in PSCs and Diminish Macromolecular Permeability of 3D-PDAC Fibrotic Tissues via a DDR1/2-Dependent Mechanism

Incidentally, we found that the MEK inhibitor trametinib strongly induces the protein (**Figure** 2A–C, Supporting Information) and mRNA (Figure 2D,E) expression of collagen I in PSCs. The induction of collagen I by trametinib is not a specific feature to this compound but rather a general characteristic of MEK inhibitors, as two other MEK inhibitors, CI-1040 (Figure S5A–C, Supporting Information) and U0126 (Figure S5D–F, Supporting Information), also up-regulated collagen I expression in PSCs. Higher doses of MEK inhibitors understandably suppressed PSC cell growth, albeit at substantially higher concentrations than required to inhibit growth of PDAC tumor cells (Figure S6A–C, Supporting Information).

Of note, trametinib diminished macromolecular permeability of 3D-PDAC fibrotic tissues at 10 nM in PSC #1 and 10–30 nM in PSC #2 without decreasing 3D-PDAC fibrotic tissue thickness (Figure 2F–I). Trametinib administered 2 mg daily, as previously tested in a phase II clinical trial against PDAC,[18] has a reported serum C_{max} of 14.0–32.9 ng mL^{-1}.[26] This equates to 22.7–53.5 nM, which suggests that trametinib at clinically relevant concentrations may exacerbate the fibrotic barrier. On the other hand, higher concentrations (100–1000 nM) of trametinib increased macromolecular permeability (Figure S6D–G, Supporting Information). This is presumably due to its inhibitory effect on cell proliferation/viability (Figure S6A–C, Supporting Information), which corresponds with the tendency for tissue thickness to decrease at the highest concentration tested (1000 nM; Figure S6D,E, Supporting Information).

To establish whether a causative relationship exists between up-regulated collagen I levels and diminished macromolecular permeability induced by trametinib at clinically relevant concentrations, we compared 3D-PDAC fibrotic tissues constructed from PSCs treated with a 1:1 mixture of siRNAs against *COL1A1* and *COL1A2* (siCOL1A1+2) to target both constituent chains of collagen I (two α1 chains + one α2 chain, encoded by *COL1A1* and *COL1A2* genes, respectively) versus a control (ctrl) siRNA. First, we confirmed successful knockdown of collagen I expression by siCOL1A1+2 treatment in PSCs (Figure S7A–D, Supporting Information). In line with the importance of collagen I accumulation in generation of the fibrotic barrier, siCOL1A1+2 treatment increased macromolecular permeability at baseline although the thicknesses of 3D-PDAC fibrotic tissues were similar (Figure S7E–H, Supporting Information). Importantly, while trametinib diminished macromolecular permeability in 3D-PDAC fibrotic tissues constructed from ctrl siRNA-treated PSCs, permeability was not significantly diminished by trametinib in 3D-PDAC fibrotic tissues constructed from siCOL1A1+2-treated PSCs (Figure S7G,H, Supporting Information).

We next wondered whether DDR1/2 inhibition, which decreased collagen I production in PSCs and enhanced macromolecular permeability of 3D-PDAC fibrotic tissues at baseline (Figure 1), could counteract the effect of trametinib. Indeed,

Figure 1. Pharmacological inhibition of DDR1/2 attenuates collagen I expression by PSCs to enhance macromolecular permeability of 3D-PDAC fibrotic tissues. A) Representative immunofluorescent staining for collagen I (green) and β-tubulin (red) in PSCs treated with the DDR1/2 inhibitor VU-6015929. Nuclei (blue) were stained with Hoechst 33342. B,C) Quantification of mean collagen I fluorescence per cell using CellProfiler[24] in VU-6015929-treated PSCs. Aggregated data for three independently performed experiments are shown in distinct colors as superplots:[25] small data points in the background demonstrate quantified values of individual cells, large data points in the foreground show the per experiment mean, together with error bars indicating standard deviation (SD) of the means. D) Maximum intensity projection images of VU-6015929-treated 3D-PDAC fibrotic tissues immunofluorescently stained for collagen I. Insets show insert-wide images. E,F) Insert-wide quantification of mean collagen I fluorescence of VU-6015929-treated 3D-PDAC fibrotic tissues. G–J) Representative 3D-reconstructed images (G,I) and measured thickness (H,J) of VU-6015929-treated 3D-PDAC fibrotic tissues. $n = 8$ measurements. K,L) Permeability of VU-6015929-treated 3D-PDAC fibrotic tissues to fluorescein isothiocyanate (FITC)-labeled dextran with an average molecular weight of 2000 kDa. M) Schematic depiction of assay assessing therapeutic effect of permeated clinical nanomedicines on PDAC cancer cells. N–Q) Effect of Doxil (N,O) and Abraxane (P,Q) which permeated the 3D-PDAC fibrotic tissues on MiaPaCa-2 proliferation was compared to direct administration of the respective nanomedicine (second row). Cell numbers are shown relative to untreated MiaPaCa-2 cells (No trt; first row). Insets depict representative crystal violet stains. Scale bars = 100 μm, except in insets of (D) where scale bars = 1 mm and 3D-reconstructed images in (G) and (I) where vertical scale bars = 20 μm. One-way analysis of variance (ANOVA) with *post hoc* Dunnett's multiple comparisons test was performed with 0 μM as the reference condition, and *n.s.*, *, **, ***, and **** denote not significant, $p < 0.05$, $p < 0.01$, $p < 0.001$, and $p < 0.0001$, respectively.

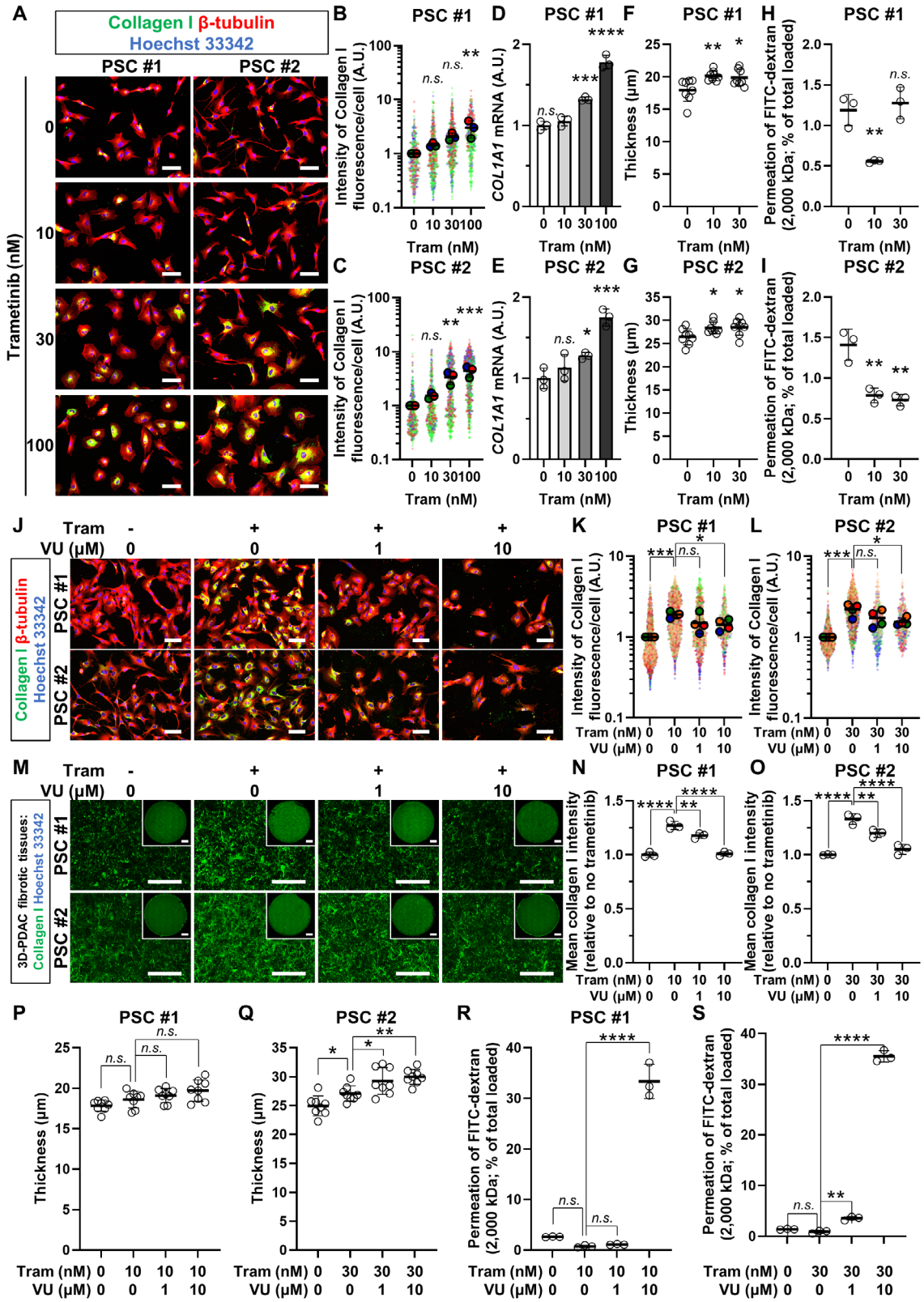

VU-6015929 suppressed collagen I up-regulation induced by trametinib in PSCs in 2D (Figure 2J–L) as well as in 3D-PDAC fibrotic tissues (Figure 2M–O). Moreover, VU-6015929 concomitantly reversed the trametinib-induced diminution of macromolecular permeability without decreasing 3D-PDAC fibrotic tissue thickness (Figure 2P–S). These results altogether suggest that at clinically relevant concentrations, MEK inhibitors induce collagen I up-regulation in PSCs to impede macromolecular permeability in 3D-PDAC fibrotic tissues via a DDR1/2-dependent mechanism.

2.3. Targeting of DDR1 is Sufficient to Enhance Macromolecular Permeability of 3D-PDAC Fibrotic Tissues

The above results suggest the utility of targeting DDR1/2 to enhance macromolecular permeability of fibrotic tissue in PDAC. To test this notion further, we assessed two additional DDR inhibitors (**Figure 3**A): DDR1-IN-1 (more specific to DDR1[27]) and WRG-28 (more specific to DDR2[28]). Higher concentrations (>1 μM) of both DDR1-IN-1 and WRG-28 decreased PSC cell growth (Figure S1E–L, Supporting Information). Interestingly, while neither compound affected 3D-PDAC fibrotic tissue thickness (Figure 3B–E), DDR1-IN-1 at 5 μM enhanced macromolecular permeability (Figure 3F,G), while in contrast an equal concentration of WRG-28 did not (Figure 3H,I).

These results implicated the effectiveness of specifically targeting DDR1 rather than DDR2 in enhancing macromolecular permeability. We thus turned to isoform-specific knockdown of DDRs with siRNAs (Figure S8A–D, Supporting Information) to establish the differential roles of DDR1 versus DDR2. Knockdown of either *DDR1* or *DDR2* somewhat diminished PSC cell growth, with *DDR1* knockdown tending to have a stronger effect (Figure S1M–P, Supporting Information). Knockdown of neither DDRs decreased 3D-PDAC fibrotic tissue thickness (Figure 3J,K). However, *DDR1* knockdown enhanced macromolecular permeability whereas *DDR2* knockdown did not (Figure 3L,M), corroborating the results obtained with DDR1-IN-1 and WRG-28. Moreover, consistent with the effect on macromolecular permeability, *DDR1* knockdown diminished collagen I expression in PSCs by ≈20% whereas *DDR2* knockdown had no significant effect (Figure 3N–P). Altogether, these results suggest that targeting of DDR1 suffices to diminish collagen I expression in PSCs to enhance macromolecular permeability of fibrotic tissues.

2.4. Pharmacological Inhibition of PI3K Attenuates Collagen I Expression by PSCs and Enhances Macromolecular Permeability of 3D-PDAC Fibrotic Tissues

We next sought to elucidate the signaling mechanisms downstream of DDRs involved in regulating collagen I expression by PSCs as well as the macromolecular permeability of fibrotic tissues. Inspired by a recent report that DDR1 signaling through the pro-inflammatory transcription factor nuclear factor-kappa B (NFκB) promotes PDAC progression,[29] we treated PSCs with the NFκB inhibitor BAY 11-7082 (Figure S9A–D, Supporting Information). BAY 11-7082 treatment of up to 3 μM did not suppress 3D-PDAC fibrotic tissue thickness (Figure S9E,F, Supporting Information) nor did it reliably improve macromolecular permeability of the 3D-PDAC fibrotic tissues, as significant improvement was observed only in PSC #1, but not in PSC #2 (Figure S9G,H, Supporting Information). Concentrations above 3 μM strongly suppressed PSC cell growth (≈90% reduction at 10 μM) and were not testable (Figure S9A–D, Supporting Information).

We next turned to the PI3K/AKT/mTOR pathway, since it is a known downstream effector of DDR1,[30] and dysregulation of PI3K activity was previously implicated in the pathogenesis of chronic pancreatitis.[31] To this end, we first assessed whether VU-6015929 affects the phosphorylation of ribosomal protein S6 (p-S6), given that S6 is a well-characterized phosphorylation substrate indicative of mTOR activity.[32] Indeed, VU-6015929 decreased p-S6 levels (**Figure 4**A–C), suggesting the involvement of the PI3K/AKT/mTOR pathway downstream of DDR1 in PSCs. Further supporting this notion, the PI3K inhibitor LY294002 diminished both p-S6 levels (Figure 4D–F) and collagen I expression by PSCs in 2D (Figure 4G–I). LY294002 also diminished collagen I deposition in 3D-PDAC fibrotic tissues (Figure 4J–L). LY294002 at these concentrations moderately diminished PSC cell growth (Figure S10A–D, Supporting Information), but did not decrease 3D-PDAC fibrotic tissue thickness (Figure 4M,N). Macromolecular permeability was nonetheless enhanced by LY294002 in a dose-dependent manner (Figure 4O,P).

Based on our above observation that VU-6015929 is effective in enhancing macromolecular permeability of 3D-PDAC fibrotic tissues at baseline (Figure 1), as well as in reversing the fibrotic barrier exacerbated by trametinib (Figure 2), we wondered whether similar downstream effectors are at play. Indeed, LY294002 effectively reversed collagen I induced by trametinib in

Figure 2. MEK inhibitors induce collagen I expression in PSCs and diminish macromolecular permeability of 3D-PDAC fibrotic tissues via a DDR1/2-dependent mechanism. A) Immunofluorescent staining for collagen I (green) and β-tubulin (red) in PSCs treated with the MEK inhibitor trametinib (tram). Nuclei (blue) were stained with Hoechst 33342. B,C) Mean collagen I fluorescence per cell in trametinib-treated PSCs. D,E) Reverse transcription-quantitative polymerase chain reaction (RT-qPCR) analyses of *COL1A1* mRNA expression by trametinib-treated PSCs. F–I) Thickness (F,G) and permeability to 2000 kDa FITC-dextran (H,I) of trametinib-treated 3D-PDAC fibrotic tissues. J) Immunofluorescent staining for collagen I (green) and β-tubulin (red) in PSCs treated with VU-6015929 (VU) and trametinib. Nuclei (blue) were stained with Hoechst 33342. Scale bars = 100 μm. K,L) Mean collagen I fluorescence per cell in PSCs upon VU-6015929 and trametinib treatment. M) Maximum intensity projection images of 3D-PDAC fibrotic tissues treated with VU-6015929 and trametinib immunofluorescently stained for collagen I. Insets show insert-wide images. N,O) Insert-wide mean collagen I fluorescence of 3D-PDAC fibrotic tissues treated with VU-6015929 and trametinib. P–S) Thickness (P,Q) and permeability to 2000 kDa FITC-dextran (R,S) of 3D-PDAC fibrotic tissues treated with VU-6015929 and trametinib. In all experiments, trametinib was administered at 10 nM for PSC #1 and at 30 nM for PSC #2. $n = 8$ in all thickness measurements. Scale bars = 100 μm, except in insets of (M) where scale bars = 1 mm. One-way ANOVA with *post hoc* Dunnett's multiple comparisons test was performed with 0 nM trametinib as the reference condition, and *n.s.*, *, **, ***, and **** denote not significant, $p < 0.05$, $p < 0.01$, $p < 0.001$, and $p < 0.0001$, respectively.

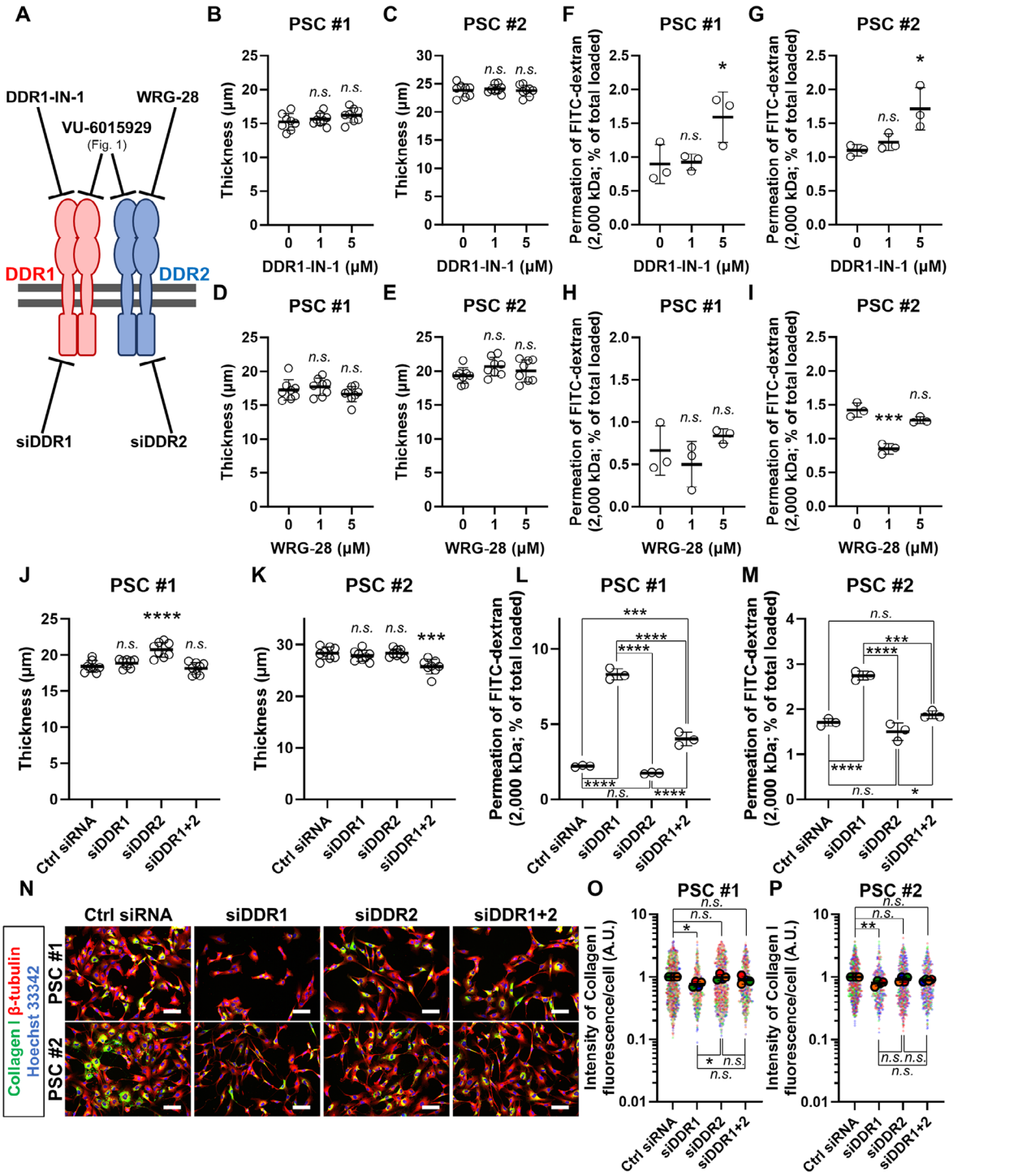

Figure 3. Targeting of DDR1 is sufficient to enhance macromolecular permeability of 3D-PDAC fibrotic tissues. A) Schematic figure showing targets of pharmacological inhibitors and siRNA knockdowns performed. B–I) Thickness (B–E) and permeability to 2000 kDa FITC-dextran (F–I) of 3D-PDAC fibrotic tissues treated with the DDR1 inhibitor DDR1-IN-1 (B,C,F,G) or DDR2 inhibitor WRG-28 (D,E,H,I). J–M) Thickness (J,K) and permeability to 2000 kDa FITC-dextran (L,M) of 3D-PDAC fibrotic tissues constructed from PSCs treated with an siRNA targeting DDR1 (siDDR1), DDR2 (siDDR2), or a 1:1 mixture of the two (siDDR1+2) versus control siRNA (ctrl siRNA). N) Immunofluorescent staining for collagen I (green) and β-tubulin (red) in PSCs treated with ctrl siRNA, siDDR1, siDDR2, or siDDR1+2. Nuclei (blue) were stained with Hoechst 33342. Scale bars = 100 μm. O,P) Mean collagen I fluorescence per cell in PSCs treated as in (N). $n = 8$ in all thickness measurements. In (L), (M), (O), and (P), one-way ANOVA with *post hoc* Tukey's multiple comparisons test was performed. In all other graphs, one-way ANOVA with *post hoc* Dunnett's multiple comparisons test was performed with 0 μM or ctrl siRNA as the reference condition. In all graphs, *n.s.*, *, **, ***, and **** denote not significant, $p < 0.05$, $p < 0.01$, $p < 0.001$, and $p < 0.0001$, respectively.

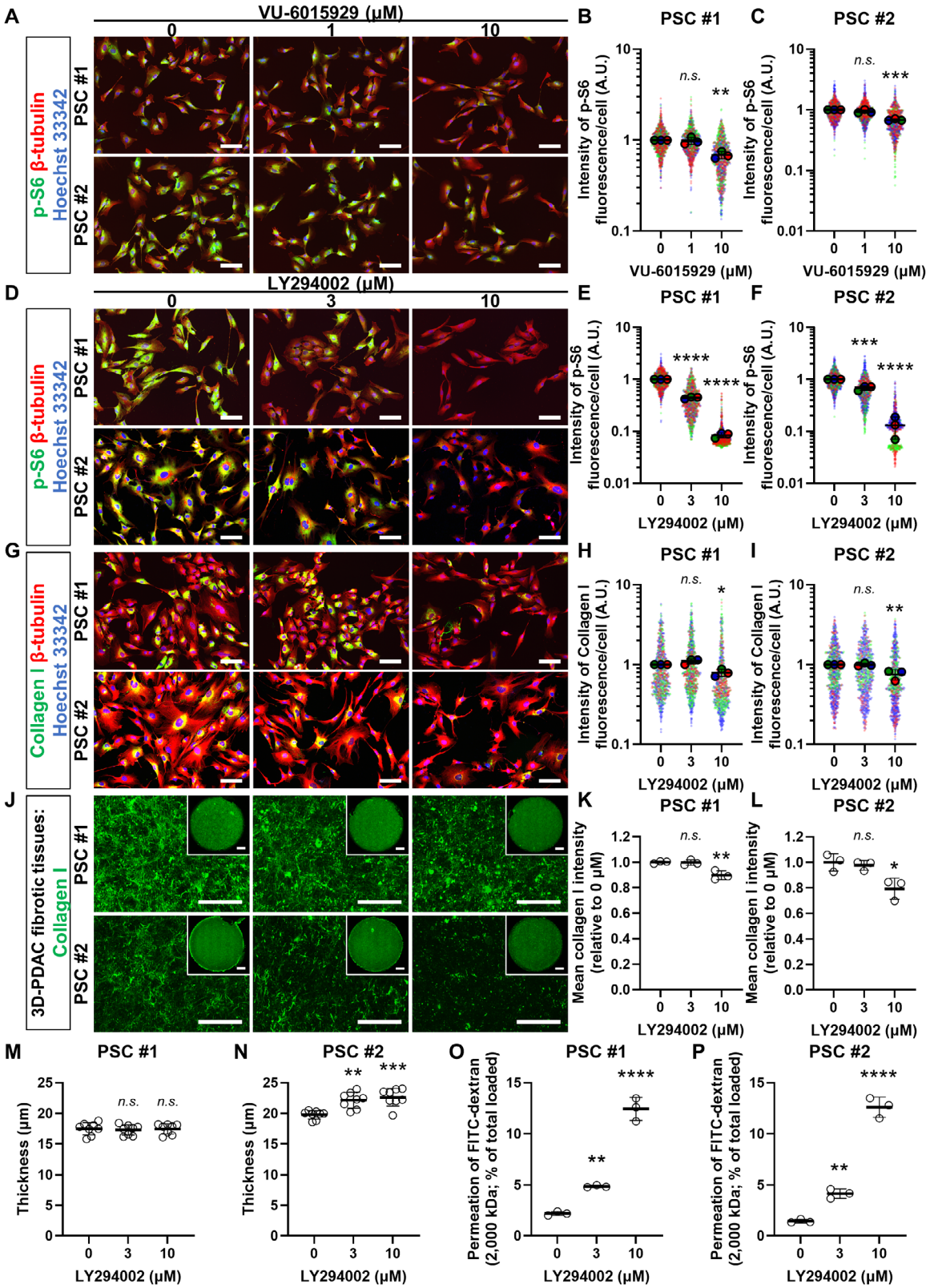

PSCs in 2D (Figure S11A–C, Supporting Information). Though 3D-PDAC fibrotic tissue thickness was not appreciably altered (Figure S11D,E, Supporting Information), LY294002 enhanced macromolecular permeability even in the presence of trametinib (Figure S11F,G, Supporting Information).

2.5. Pharmacological Inhibition of AKT Attenuates Collagen I Expression by PSCs and Enhances Macromolecular Permeability of 3D-PDAC Fibrotic Tissues

To further assess the involvement of the PI3K/AKT/mTOR pathway, we utilized the pan-AKT inhibitor MK2206.[33] As with LY294002, MK2206 dose-dependently diminished collagen I expression by PSCs in 2D (**Figure 5**A–C) and collagen I deposition in 3D-PDAC fibrotic tissues (Figure 5D–F). MK2206 at these concentrations somewhat diminished PSC cell growth (Figure S10E–H, Supporting Information) but did not decrease 3D-PDAC fibrotic tissue thickness (Figure 5G,H). Macromolecular permeability was enhanced by MK2206 dose-dependently (Figure 5I,J). We furthermore asked whether MK2206 could reverse the changes induced by trametinib. Indeed, MK2206 effectively reversed trametinib-induced collagen I in PSCs (Figure S11H–J, Supporting Information). MK2206 did not appreciably alter 3D-PDAC fibrotic tissue thickness (Figure S11K,L, Supporting Information), but enhanced macromolecular permeability even in the presence of trametinib (Figure S11M,N, Supporting Information).

Interestingly, despite MK2206 diminishing collagen I expression by PSCs and enhancing macromolecular permeability, it minimally affected p-S6 levels (Figure 5K–M). Although diminution of p-S6 levels by VU-6015929 (Figure 4A–C) led us to assess and confirm the involvement of PI3K/AKT/mTOR, these results suggested that the changes in p-S6 levels per se are not directly correlated with collagen I expression or macromolecular permeability.

2.6. Pharmacological Inhibition of mTOR Attenuates Collagen I Expression by PSCs and Enhances Macromolecular Permeability of 3D-PDAC Fibrotic Tissues

Having confirmed the effect of PI3K (Figure 4) and AKT (Figure 5) inhibition in diminishing collagen I expression by PSCs and enhancing macromolecular permeability of fibrotic tissues, we finally turned to mTOR. As expected, the mTOR inhibitor AZD8055[34] reduced p-S6 levels (**Figure 6**A–C). AZD8055 diminished collagen I expression by PSCs in 2D (Figure 6D–F) as well as collagen I deposition in 3D-PDAC fibrotic tissues (Figure 6G–I). Though AZD8055 dose-dependently diminished PSC cell growth (Figure S10I–L, Supporting Information), AZD8055 at concentrations enough to reduce collagen I expression (0.1 or 0.3 μM) did not decrease 3D-PDAC fibrotic tissue thickness (Figure 6J,K). Macromolecular permeability was however enhanced by AZD8055 at these concentrations (Figure 6L,M).

Here, too, we assessed the efficacy of AZD8055 against the changes induced by trametinib. Indeed, AZD8055 effectively reversed collagen I induced by trametinib in PSCs (Figure S11O–Q, Supporting Information). Thickness of 3D-PDAC fibrotic tissues treated with both trametinib and AZD8055 were somewhat diminished compared to trametinib alone, but overall comparable to tissues treated with neither (Figure S11R,S, Supporting Information). Nonetheless, AZD8055 enhanced macromolecular permeability, even in the presence of trametinib, to levels higher than baseline (Figure S11T,U, Supporting Information). Altogether, the above results suggest that DDR1 signals through the PI3K/AKT/mTOR pathway to induce collagen I expression in PSCs to impede macromolecular permeability of fibrotic tissues (Figures 4–6), and furthermore that this pathway is exacerbated by MEK inhibition (Figure S11, Supporting Information).

2.7. Knockdown of RPTOR and/or RICTOR Fails to Attenuate Collagen I Expression by PSCs or Improve Macromolecular Permeability of 3D-PDAC Fibrotic Tissues

Having established the involvement of the DDR1/PI3K/AKT/mTOR pathway, we sought to further clarify the nature of mTOR signaling, as mTOR usually functions as a component of two canonical complexes, mTOR complexes (mTORC) 1 and mTORC2 (**Figure 7**A), with non-redundant functions.[32] We hypothesized that mTORC2 is predominantly involved, as mTORC1 regulates p-S6 levels through phosphorylation-dependent regulation of p70 S6 kinase 1, while mTORC2 does not.[32] We reasoned that a predominant role of mTORC2 would explain the disjunction between changes in p-S6 levels versus changes in collagen I expression or macromolecular permeability.

To assess this, we performed knockdown of *RPTOR* (encoding Raptor, a requisite component of mTORC1; Figure S8E,F, Supporting Information) and/or *RICTOR* (a requisite component of mTORC2; Figure S8G,H, Supporting Information). As expected, knockdown of *RPTOR*, but not *RICTOR*, reduced p-S6 levels in PSCs (Figure 7B–D). Surprisingly, however, knockdown of neither *RPTOR* nor *RICTOR* decreased collagen I expression by PSCs (Figure 7E–G). PSC cell growth was comparably diminished by knockdown of either *RPTOR*, *RICTOR*, or both combined (Figure S12A–D, Supporting Information).

Figure 4. Pharmacological inhibition of PI3K attenuates collagen I expression by PSCs and enhances macromolecular permeability of 3D-PDAC fibrotic tissues. A) Immunofluorescent staining for phospho-S6 (p-S6; green) and β-tubulin (red) in PSCs treated with VU-6015929. Nuclei (blue) were stained with Hoechst 33342. B,C) Mean p-S6 fluorescence per cell in VU-6015929-treated PSCs. D) Immunofluorescent staining for p-S6 (green) and β-tubulin (red) in PSCs treated with the PI3K inhibitor LY294002. Nuclei (blue) were stained with Hoechst 33342. Scale bars = 100 μm. E,F) Mean p-S6 fluorescence per cell in LY294002-treated PSCs. G) Immunofluorescent staining for collagen I (green) and β-tubulin (red) in LY294002-treated PSCs. Nuclei (blue) were stained with Hoechst 33342. H,I) Mean collagen I fluorescence per cell in LY294002-treated PSCs. J) Maximum intensity projection images of LY294002-treated 3D-PDAC fibrotic tissues immunofluorescently stained for collagen I. Insets show insert-wide images. K,L) Insert-wide mean collagen I fluorescence of LY294002-treated 3D-PDAC fibrotic tissues. M–P) Thickness (M,N) and permeability to 2000 kDa FITC-dextran (O,P) of LY294002-treated 3D-PDAC fibrotic tissues. $n = 8$ thickness measurements. Scale bars = 100 μm, except in insets of (J) where scale bars = 1 mm. One-way ANOVA with *post hoc* Dunnett's multiple comparisons test was performed with 0 μM as the reference condition, and *n.s.*, *, **, ***, and **** denote not significant, $p < 0.05$, $p < 0.01$, $p < 0.001$, and $p < 0.0001$, respectively.

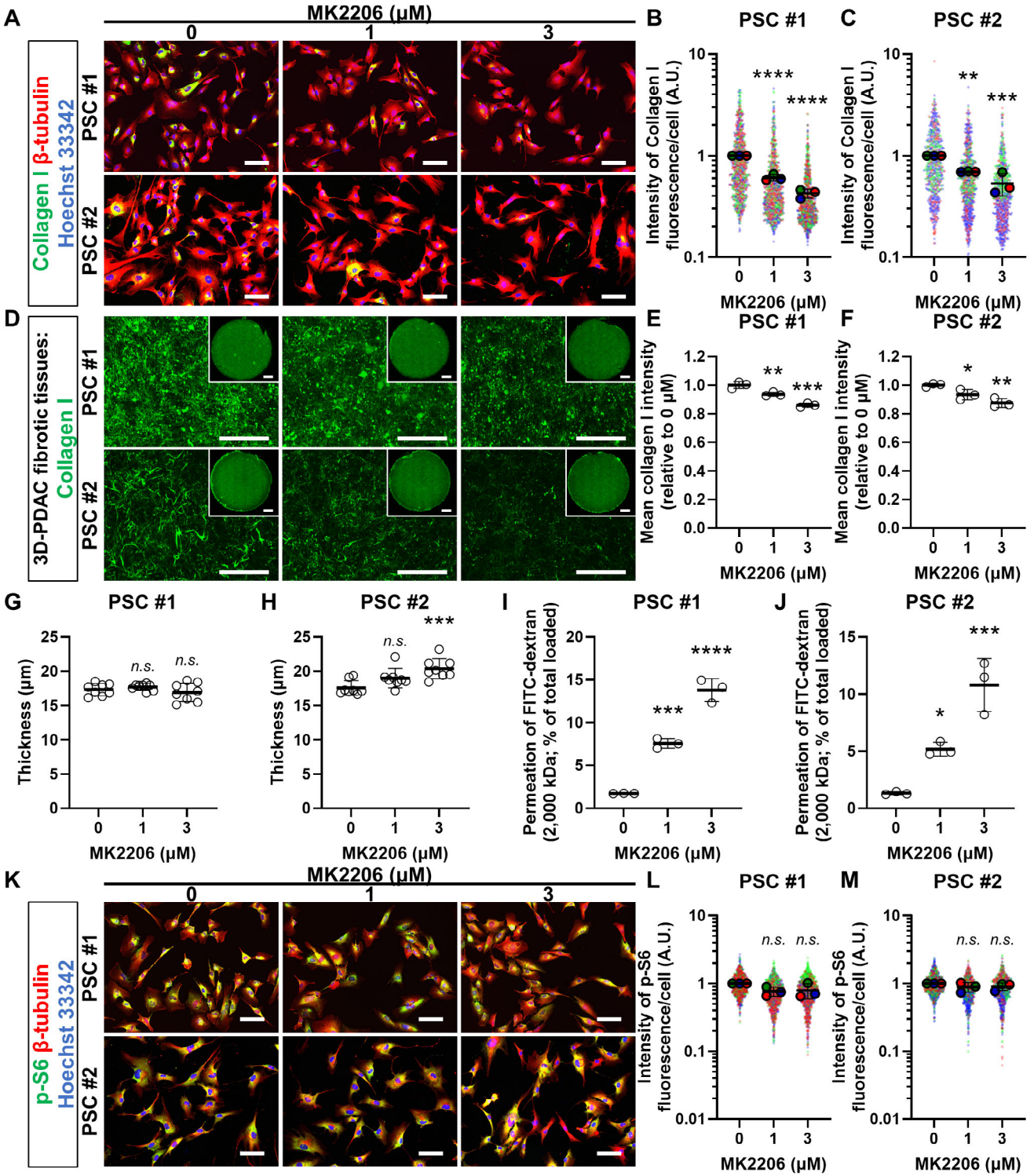

Figure 5. Pharmacological inhibition of AKT attenuates collagen I expression by PSCs and enhances macromolecular permeability of 3D-PDAC fibrotic tissues. A) Immunofluorescent staining for collagen I (green) and β-tubulin (red) in PSCs treated with the AKT inhibitor MK2206. Nuclei (blue) were stained with Hoechst 33342. B,C) Mean collagen I fluorescence per cell in MK2206-treated PSCs. D) Maximum intensity projection images of MK2206-treated 3D-PDAC fibrotic tissues immunofluorescently stained for collagen I. Insets show insert-wide images. E,F) Insert-wide mean collagen I fluorescence of MK2206-treated 3D-PDAC fibrotic tissues. G–J) Thickness (G,H) and permeability to 2000 kDa FITC-dextran (I,J) of MK2206-treated 3D-PDAC fibrotic tissues. $n = 8$ thickness measurements. K) Immunofluorescent staining for p-S6 (green) and β-tubulin (red) in MK2206-treated PSCs. Nuclei (blue) were stained with Hoechst 33342. L,M) Mean p-S6 fluorescence per cell in MK2206-treated PSCs. Scale bars = 100 μm, except in insets of (D) where scale bars = 1 mm. One-way ANOVA with *post hoc* Dunnett's multiple comparisons test was performed with 0 μM as the reference condition, and *n.s.*, *, **, ***, and **** denote not significant, $p < 0.05$, $p < 0.01$, $p < 0.001$, and $p < 0.0001$, respectively.

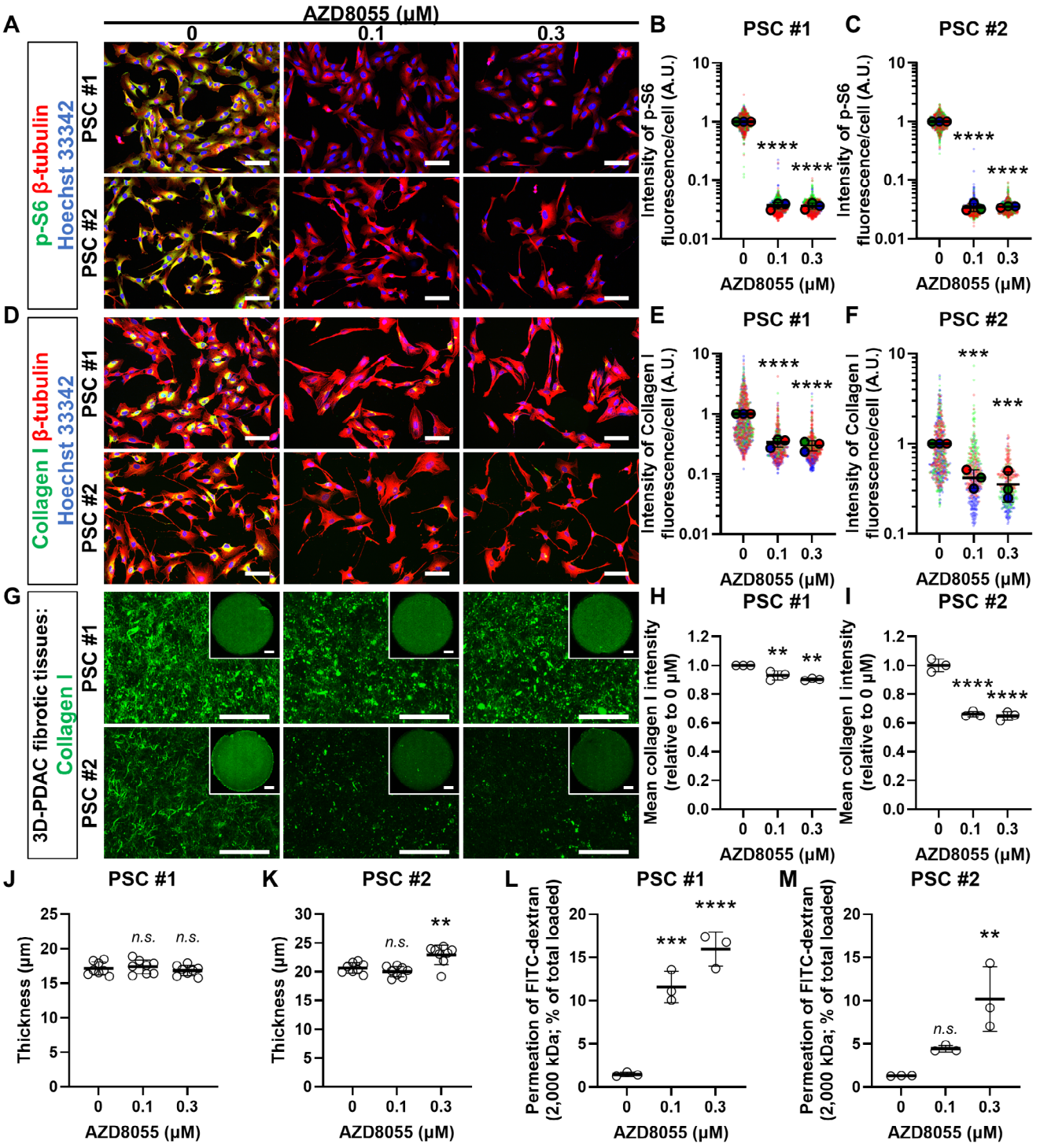

Figure 6. Pharmacological inhibition of mTOR attenuates collagen I expression by PSCs and enhances macromolecular permeability of 3D-PDAC fibrotic tissues. A) Immunofluorescent staining for p-S6 (green) and *β*-tubulin (red) in PSCs treated with the mTOR inhibitor AZD8055. Nuclei (blue) were stained with Hoechst 33342. B,C) Mean p-S6 fluorescence per cell in AZD8055-treated PSCs. D) Immunofluorescent staining for collagen I (green) and *β*-tubulin (red) in AZD8055-treated PSCs. Nuclei (blue) were stained with Hoechst 33342. E,F) Mean collagen I fluorescence per cell in AZD8055-treated PSCs. G) Maximum intensity projection images of AZD8055-treated 3D-PDAC fibrotic tissues immunofluorescently stained for collagen I. Insets show insert-wide images. H,I) Insert-wide mean collagen I fluorescence of AZD8055-treated 3D-PDAC fibrotic tissues. J–M) Thickness (J,K) and permeability to 2000 kDa FITC-dextran (L,M) of AZD8055-treated 3D-PDAC fibrotic tissues. $n = 8$ thickness measurements. Scale bars = 100 μm, except in insets of (G) where scale bars = 1 mm. One-way ANOVA with *post hoc* Dunnett's multiple comparisons test was performed with 0 μM as the reference condition, and *n.s.*, **, ***, and **** denote not significant, $p < 0.01$, $p < 0.001$, and $p < 0.0001$, respectively.

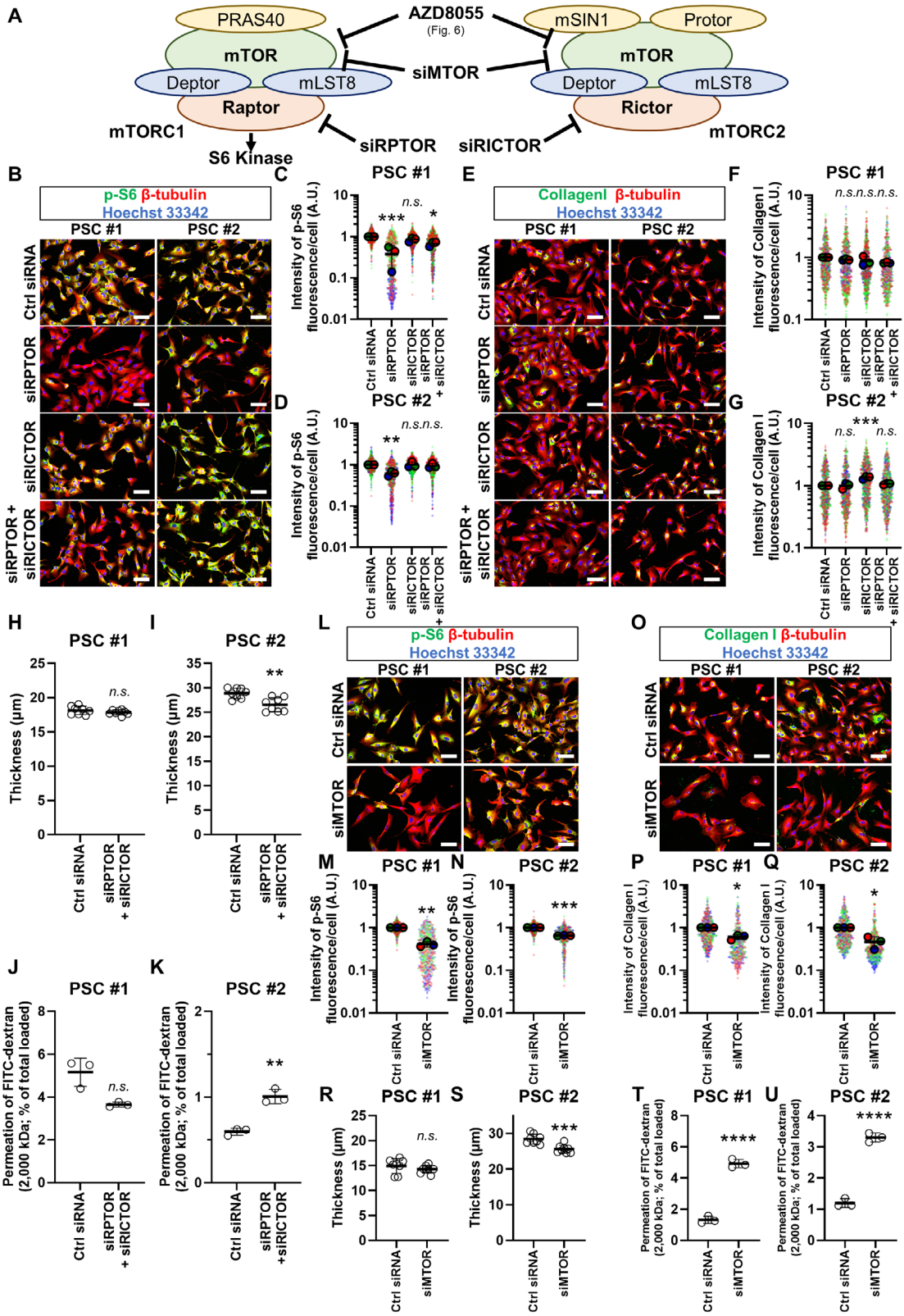

Moreover, combined knockdown of *RPTOR* and *RICTOR* did not lead to consistent changes in the thickness or macromolecular permeability of 3D-PDAC fibrotic tissues (Figure 7H–K).

The lack of effect of both *RPTOR* and *RICTOR* knockdown first led us to suspect mTOR-independent off-target pharmacological effects of AZD8055, despite its reportedly highly selective activity profile.[34] However, as with AZD8055 treatment, *MTOR* knockdown (Figure S8I,J, Supporting Information) decreased p-S6 levels (Figure 7L–N) and collagen I expression by PSCs (Figure 7O–Q). Moreover, *MTOR* knockdown decreased PSC cell growth (Figure S12E–H, Supporting Information). Though *MTOR* knockdown did not consistently affect 3D-PDAC fibrotic tissue thickness (Figure 7R,S), macromolecular permeability was nonetheless enhanced (Figure 7T,U). Overall, AZD8055 treatment and *MTOR* knockdown yielded consistent, similar results. This suggests that mTOR is indeed involved in the regulation of collagen I expression by PSCs and macromolecular permeability of 3D-PDAC fibrotic tissues, albeit in an mTORC1/2-independent manner.

2.8. Combined Knockdown of MEAK7 and GIT1 Attenuates Collagen I Expression by PSCs and Enhances Macromolecular Permeability of 3D-PDAC Fibrotic Tissues

Although less characterized than the canonical mTORC1 and mTORC2, alternative mTORCs (**Figure** 8A) have recently been reported. For example, an alternative mTORC characterized by the interaction of mTOR with the ETS variant transcription factor 7 (ETV7),[35] as well as another by interaction of MTOR associated protein, Eak-7 homolog (MEAK7) and DNA-PKcs have been reported.[36] These alternative mTORCs have been named mTORC3 and mTORC4, respectively.[37] Proteomic analysis has also uncovered an mTORC characterized by mTOR interaction with G protein-coupled receptor kinase interacting ArfGAP 1 (GIT1).[38]

Given the above results implicating Raptor (mTORC1) and Rictor (mTORC2)-independent involvement of mTOR in collagen I expression by PSCs and macromolecular permeability of 3D-PDAC fibrotic tissues (Figure 6), we wondered whether alternative mTORCs might be involved. To test this notion, we assessed *ETV7*, *MEAK7*, or *GIT1* knockdown in PSCs (Figure S8K–P, Supporting Information). Only *GIT1* knockdown consistently decreased PSC cell growth (Figure S12I–L, Supporting Information). None of the knockdowns significantly diminished p-S6 levels (Figure 8B–D) or collagen I expression by PSCs (Figure 8E–G).

Because targeting individual mTORCs alone did not recapitulate the effects seen upon targeting mTOR, we next turned to combinatorial targeting of mTORCs. Given the ineffectiveness of combined *RPTOR* and *RICTOR* knockdown (Figure 7E–G,J,K), we asked whether combinatorial targeting of the alternative mTORCs could be effective. Specifically, we investigated the effect of combined *MEAK7* and *GIT1* knockdown for the following two reasons. First, *MEAK7* or *GIT1* knockdown, though statistically not significant, tended to reduce collagen I expression by about 20% in PSCs (Figure 8E–G). Second, *GIT1* knockdown upregulated *MEAK7* expression (Figure S8M,N, Supporting Information), which would presumably weaken its inhibitory effect on collagen I expression.

Consistent with knockdown of *MEAK7* or *GIT1* alone, combined *MEAK7* and *GIT1* knockdown did not reduce p-S6 levels (Figure 8H–J). In contrast, combined *MEAK7* and *GIT1* knockdown significantly decreased collagen I expression by 50–60% in PSCs (Figure 8K–M), an effect larger than either knockdown alone (Figure 8E–G). Collagen I deposition in 3D-PDAC fibrotic tissues was also significantly diminished by combined *MEAK7* and *GIT1* knockdown (Figure 8N–P). Furthermore, while combined *MEAK7* and *GIT1* knockdown diminished PSC cell growth (Figure S12M–P, Supporting Information), 3D-PDAC fibrotic tissue thickness was not consistently affected (Figure 8Q,R). Nonetheless, combined *MEAK7* and *GIT1* knockdown enhanced macromolecular permeability of the 3D-PDAC fibrotic tissues (Figure 8S,T). The above results together suggest that the effects observed upon pharmacological or siRNA-mediated targeting of mTOR can be explained, at least in part, by its combined effects on alternative mTORCs involving MEAK7 and/or GIT1.

3. Discussion

We herein investigated the involvement of the collagen-activated receptor DDR in the PDAC fibrotic barrier. We show that inhibition of DDR1, but not DDR2, enhances macromolecular permeability (Figure S13, Supporting Information). Although previous studies focused on excessively deposited collagen as a physical barrier,[2,3,12] our results highlight an additional, nonstructural role of collagen in impeding macromolecular drug delivery. Specifically, DDR1-mediated collagen signaling promotes fibrotic phenotypes in PSCs, forming a vicious cycle driving the fibrotic barrier. This suggests that focusing on cellular

Figure 7. Knockdown of *RPTOR* and/or *RICTOR* fails to attenuate collagen I expression by PSCs or improve macromolecular permeability of 3D-PDAC fibrotic tissues. A) Schematic depiction of canonical mTORC1 and mTORC2 components. B) Immunofluorescent staining for p-S6 (green) and β-tubulin (red) in PSCs treated with an siRNA targeting RAPTOR (siRPTOR), RICTOR (siRICTOR), a 1:1 mixture of the two siRNAs (siRPTOR + siRICTOR), or ctrl siRNA. Nuclei (blue) were stained with Hoechst 33342. C,D) Mean p-S6 fluorescence per cell in PSCs treated as in (B). E) Immunofluorescent staining for collagen I (green) and β-tubulin (red) in PSCs treated with ctrl siRNA, siRPTOR, siRICTOR, or siRPTOR + siRICTOR. Nuclei (blue) were stained with Hoechst 33342. F,G) Quantification of mean collagen I fluorescence per cell in PSCs treated as in (E). H–K) Thickness (H,I) and permeability to 2000 kDa FITC-dextran (J,K) of 3D-PDAC fibrotic tissues constructed from PSCs treated with ctrl siRNA, siRPTOR, siRICTOR, or siRPTOR + siRICTOR. L) Immunofluorescent staining for p-S6 (green) and β-tubulin (red) in PSCs treated with ctrl siRNA or an siRNA targeting MTOR (siMTOR). Nuclei (blue) were stained with Hoechst 33342. M,N) Mean p-S6 fluorescence per cell in PSCs treated as in (L). O) Immunofluorescent staining for collagen I (green) and β-tubulin (red) in PSCs treated with ctrl siRNA or siMTOR. Nuclei (blue) were stained with Hoechst 33342. P,Q) Mean collagen I fluorescence per cell in PSCs treated as in (O). R–U) Thickness (R,S) and permeability to 2000 kDa FITC-dextran (T,U) of 3D-PDAC fibrotic tissues constructed from PSCs treated with ctrl siRNA or siMTOR. $n = 8$ for all thickness measurements. Scale bars = 100 µm. One-way ANOVA with *post hoc* Dunnett's multiple comparisons test was performed with ctrl siRNA as the reference condition in (C), (D), (F), and (G). In all other graphs, Student's un-paired *t*-test with Welch's correction was performed. In all graphs, *n.s.*, *, **, ***, and **** denote not significant, $p < 0.05$, $p < 0.01$, $p < 0.001$, and $p < 0.0001$, respectively.

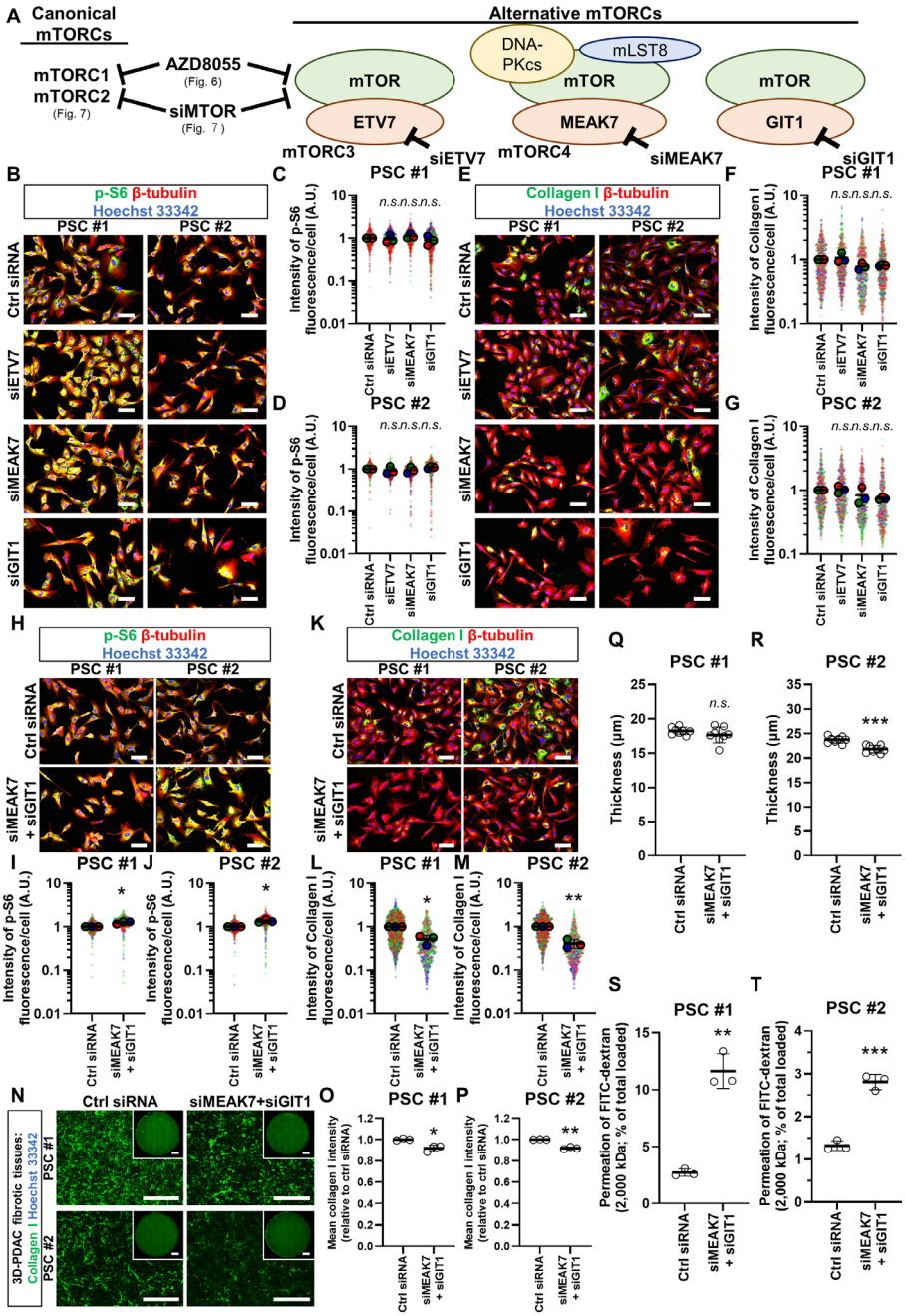

Figure 8. Combined knockdown of MEAK7 and GIT1 attenuates collagen I expression by PSCs and enhances macromolecular permeability of 3D-PDAC fibrotic tissues. A) Schematic depiction of alternative mTORC components. B) Immunofluorescent staining for p-S6 (green) and β-tubulin (red) in PSCs treated with an siRNA targeting ETV7 (siETV7), MEAK7 (siMEAK7), GIT1 (siGIT1), or ctrl siRNA. Nuclei (blue) were stained with Hoechst 33342. C,D) Mean p-S6 fluorescence per cell in PSCs treated as in (B). E) Immunofluorescent staining for collagen I (green) and β-tubulin (red) in PSCs treated with ctrl siRNA, siETV7, siMEAK7, or siGIT1. Nuclei (blue) were stained with Hoechst 33342. F,G) Mean collagen I fluorescence per cell in PSCs treated as in (E). H) Immunofluorescent staining for p-S6 (green) and β-tubulin (red) in PSCs treated with ctrl siRNA or a 1:1 mixture of siMEAK7 and siGIT1 (siMEAK + siGIT1). Nuclei (blue) were stained with Hoechst 33342. I,J) Mean p-S6 fluorescence per cell in PSCs treated as in (H). K) Immunofluorescent staining for collagen I (green) and β-tubulin (red) in PSCs treated with ctrl siRNA or siMEAK7 + siGIT1. Nuclei (blue) were stained with Hoechst 33342. L,M) Mean collagen I fluorescence per cell in PSCs treated as in (K). N) Maximum intensity projection images of 3D-PDAC fibrotic tissues constructed from PSCs treated with ctrl siRNA or siMEAK7 + siGIT1 and immunofluorescently stained for collagen I. Insets show insert-wide images. O,P) Insert-wide mean collagen I fluorescence of 3D-PDAC fibrotic tissues constructed as in (N). Q–T) Thickness (Q,R) and permeability to 2000 kDa FITC-dextran (S,T) of 3D-PDAC fibrotic tissues constructed from PSCs treated with ctrl siRNA or siMEAK7 + siGIT1. $n = 8$ thickness measurements. Scale bars = 100 μm, except in insets of (N) where scale bars = 1 mm. In (C), (D), (F), and (G), one-way ANOVA with *post hoc* Dunnett's multiple comparisons test was performed with ctrl siRNA as the reference condition. In all other graphs, Student's un-paired *t*-test with Welch's correction was performed. In all graphs, *n.s.*, *, **, and *** denote not significant, $p < 0.05$, $p < 0.01$, and $p < 0.001$, respectively.

signaling elicited by the ECM may offer novel therapeutic targets to enhance drug delivery through the PDAC fibrotic barrier.[3] We focused on collagen I due to its prime abundance within the PDAC tumor microenvironment,[11] but different subtypes, post-translational modifications, and conformations of collagen uniquely affect its signaling[29,39,40] and deserves detailed assessment in the future.

Ddr1 knockout in a genetically engineered murine PDAC model reportedly increased deposition of fibrillary collagen.[41] Our results seem contradictory at first glance, but this may be explained by differences between acute (inhibitors and siRNAs) versus chronic (genetic knockout) targeting of DDR1. In fact, the role of DDR2 in fibrosis is reported to differ between acute versus chronic settings.[13] Though further studies are necessary to delineate the context-dependent role of DDR1 in PDAC, our results highlight the non-redundant functions of the DDRs[13,42] and the potential of acute, DDR1-specific targeting to enhance macromolecular drug delivery in PDAC.

Furthermore, we show that diminution of PI3K/AKT/mTOR activity underlies the enhancement of macromolecular permeability upon targeting DDRs. Diminution of collagen I expression by inhibiting PI3K/AKT/mTOR agrees with a recent report of dysregulated PI3K activity in chronic pancreatitis[31] and aligns with clinical interest in targeting this pathway in pulmonary fibrosis.[43] Apart from PI3K/AKT/mTOR, DDR1 signals through other effectors such as NFκB and the mitogen-activated protein kinases (MAPKs).[30] Of note, DDR1-NFκB signaling in response to cleaved collagens was recently shown to promote PDAC progression.[29] NFκB in PSCs specifically also has been implicated in fibro-inflammatory processes of the pancreas.[44,45] However, the NFκB inhibitor BAY 11-7082 did not reliably improve macromolecular permeability in our 3D-PDAC fibrotic tissues. Other effectors of DDR signaling were not assessed and is a potential avenue of further research.

To gain deeper insight into the molecular mechanisms of fibrotic barrier generation, we also analyzed the contribution of the various mTORCs. Surprisingly, disruption of canonical mTORCs or alternative mTORCs individually were ineffective. However, combined targeting of MEAK7 and GIT1, neither of which have previously been implicated in fibrotic processes, effectively diminished collagen I expression and enhanced macromolecular permeability. The benefit of targeting MEAK7 and GIT1 together may be explained by the compensatory up-regulation of *MEAK7* upon *GIT1* knockdown. These findings highlight the intricate crosstalk and *trans*-regulation of various mTORCs and warrant further mechanistic investigation.

Additionally, we discovered that MEK inhibitors up-regulate collagen I expression in PSC at clinically relevant concentrations, paralleling a recent study on human keloidal fibroblasts.[46] Importantly, the increased expression of collagen I diminished macromolecular permeability of 3D-PDAC fibrotic tissues. This suggests that exacerbation of the fibrotic barrier by MEK inhibitors, together with acquired resistance of cancer cells,[47] may have played a role in the failure of these compounds in clinical trials against PDAC.[18] Interestingly, MEK inhibitor treatment has previously been reported to increase collagen deposition and associate with therapeutic resistance in murine models of melanoma.[48,49] Although therapy-induced changes in ECM expression/remodeling within the tumor microenvironment is gradually gaining attention,[50] our study is, to the best of our knowledge, the first to demonstrate therapy-induced exacerbation of the fibrotic barrier leading to diminished macromolecular permeability. While the exact mechanisms by which MEK inhibition drive collagen I expression remain unknown, a previous study suggests regulation of collagen I promoter activity and mRNA stability by ERK, the direct downstream target of MEK.[51] Nevertheless, we show that targeting DDR1 or its downstream effectors PI3K, AKT, or mTOR reverses MEK inhibitor-induced exacerbation of the fibrotic barrier. Targeting collagen signaling in combination with MEK inhibitors may thus be beneficial and warrant detailed future assessment. Of note, our simple and highly replicable in vitro system allows a detailed analysis of the molecular/cellular mechanisms underlying therapy-induced changes in the fibrotic barrier to identify promising targets and/or target combinations.

In summary, we demonstrate in vitro that targeting collagen I signaling through the DDR1/PI3K/AKT/mTOR pathway enhances macromolecular delivery through 3D-PDAC fibrotic tissues, both at baseline and in the context of MEK inhibitor-induced exacerbation of the fibrotic barrier. Our results suggest the potential of targeting DDR1-mediated collagen signaling to overcome fibrotic barriers to macromolecular drug delivery in PDAC and provide the rationale for further confirmation of efficacy in vivo.

4. Experimental Section

Cell Culture and Reagents: PSC #1 and PSC#2, immortalized PSC cell lines from human PDAC patients, were previously established and described.[52] PDAC cell-lines BxPC-3, Capan-2, HPAF-II, and MiaPaCa-2 cells were obtained from American Type Cell Collection (Manassas, VA, USA), and SUIT-2 from the Japanese Collection of Research Bioresources (Osaka, Japan). PSCs were maintained in Dulbecco's modified Eagle medium (Gibco/Thermo Fisher Scientific, Eugene, MA, USA) supplemented with 10% (v/v) fetal bovine serum, 1 × GlutaMAX (Gibco/Thermo Fisher Scientific), 50 U mL^{-1} penicillin, and 50 µg mL^{-1} streptomycin. BxPC-3, HPAF-II, and SUIT-2 cells were maintained in RPMI 1640 medium (Gibco/Thermo Fisher Scientific) supplemented with 10% fetal bovine serum (FBS), 50 U mL^{-1} penicillin, and 50 µg mL^{-1} streptomycin. Capan-2 cells were maintained in McCoy's 5A medium (Sigma-Aldrich, St. Louis, MO, USA) supplemented with 10% FBS, 1 × GlutaMAX, 50 U mL^{-1} penicillin, and 50 µg mL^{-1} streptomycin. MiaPaCa-2 cells were cultured in Dulbecco's modified Eagle medium supplemented with 10% FBS, 50 U mL^{-1} penicillin, and 50 µg mL^{-1} streptomycin.

All pharmacological inhibitors used in this study were prepared as dimethyl sulfoxide (DMSO) solutions and are as follows: AZD8055, BAY 11-7082, CI-1040, DDR1-IN-1, LY294002, MK2206, trametinib, U0126, VU-6015929, and WRG-28. BAY 11-7082 was obtained from Wako Pure Chemicals (Osaka, Japan) and WRG-28 from MedChemExpress (Monmouth Junction, NJ, USA). All other compounds were from Selleck Chemicals (Houston, TX, USA). Clinical nanomedicines used in this study, Doxil and Abraxane, were from Janssen Pharmaceutical K.K. (Tokyo, Japan) and Taiho Pharmaceutical Co., Ltd. (Tokyo, Japan), respectively. Abraxane was prepared, as per manufacturer instructions, as a 5 mg mL^{-1} solution in physiological saline (Otsuka Pharmaceutical Co., Ltd., Tokyo, Japan).

Cell Proliferation Assay: PSCs were seeded onto 6-well plates (BD Falcon/Corning, Corning, NY, USA; 1 × 10^5 well^{-1}) or onto 24-well plates (BD Falcon/Corning; 2 × 10^4 well^{-1}), except when assessing the effect of Doxil and Abraxane, where the seeding density was doubled. PDAC cells were seeded onto 24-well plates (2 × 10^4 well^{-1} for all cell-lines, except for Capan-2: 1 × 10^5 well^{-1}). When assessing the effect of siRNA-mediated knockdown, siRNA transfection was performed 24 h post cell

seeding as described below. The culture medium was replaced every day. When assessing pharmacological inhibitors, compounds were administered at the time of medium change. Plates were collected 72 h post cell seeding, except when assessing the effect of Doxil and Abraxane, where plates were collected at 48 h. Plates were washed once briefly with phosphate-buffered saline (PBS) then fixed with 4% (w/v) paraformaldehyde (PFA)/PBS (5 min, room temperature [RT]). Plates were again washed once briefly with PBS, then stained with 0.5% (w/v) aq. crystal violet (Tokyo Chemical Industry Co., Ltd., Tokyo, Japan) upon gentle rocking (20 min, RT). The staining solution was subsequently removed, and plates rinsed with water to remove any residual stain. Plates were then completely dried. Stained 6-well plates were photographed using a handheld camera. Stained 24-well plates were used for quantification, as described below. To extract crystal violet, equal amounts of 10% (v/v) aq. acetic acid were applied to each well, and plates were rocked gently (20 min, RT). After extraction, 100 µL well^{-1} was collected and applied onto 96-well plates (Nunc/Thermo Fisher Scientific, Roskilde, Denmark). Absorbance at 590 nm was measured using TriStar2 LB942 (Berthold Technologies, Bad Wildbad, Germany). Relative cell numbers were obtained by dividing each absorbance values by the average of the control condition (vehicle control for experiments involving pharmacological inhibitors, and ctrl siRNA for experiments involving siRNAs).

Immunofluorescent Staining and Analysis: PSCs (2×10^4 cells) were seeded onto 15 mm glass-bottom dishes (Matsunami Glass Ind., Osaka, Japan) coated with collagen (Nitta Gelatin, Osaka, Japan; Cellmatrix Type I-C; 0.1 mg mL^{-1}, >30 min at 37 °C). For experiments requiring knockdown, cells were transfected with the respective siRNAs prior to seeding onto glass-bottom dishes, as detailed below. First, 1×10^5 cells were seeded onto 6-well plates. Then, 24 h later, siRNAs (10 nM) were transfected using Lipofectamine RNAiMAX (Invitrogen/Thermo Fisher Scientific, Carlsbad, CA, USA). When performing combined knockdowns of two genes, relevant siRNAs were mixed in a 1:1 ratio, while keeping the total concentration of siRNAs administered the same as when performing individual knockdowns (10 nM). The siRNAs used in this study were pre-designed (MISSION siRNA, Sigma-Aldrich) except for the control siRNA (ctrl siRNA; sigma genosys, Tokyo, Japan; sense: GUACCGCACGUCAUUCGUAUC; anti-sense: UACGAAUGACGUGCGGUACGU). For the pre-designed siRNAs, the respective IDs supplied by the manufacturer are as follows: siCOL1A1 (SASI_Hs02_00301842), siCOL1A2 (SASI_Hs02_00301848), siDDR1 (SASI_Hs01_00165213), siDDR2 (SASI_Hs01_00022152), siGIT1 (SASI_Hs02_00317765), siETV7 (SASI_Hs01_00239852), siMEAK7 (SASI_Hs01_00247281), siMTOR (SASI_Hs02_00338641), siRICTOR (SASI_Hs02_00366683), and siRPTOR (SASI_Hs01_00048380). Cells were harvested for seeding onto glass-bottom dishes 24 h after siRNA transfection. The culture medium was replaced daily. Respective compounds were administered at the time of medium change.

Samples were collected for immunofluorescent staining 72 h after cell seeding. Cells were fixed with 4% (w/v) PFA/PBS (1 min, RT), permeabilized with 0.2% (v/v) Triton X-100/PBS (5 min, RT), and blocked with Blocking One (Nacalai tesque, Kyoto, Japan; 1–2 h, RT). Cells were then incubated overnight (O/N) at 4 °C with primary antibodies diluted in Blocking One. The primary antibodies used in this study are as follows: β-tubulin (014-25041; Wako Pure Chemicals; mouse monoclonal, clone: 10G10, 1/500 dilution), collagen I (ab183492; Abcam, Cambridge, UK; rabbit monoclonal, clone: EPR7785, 1/1000 dilution), and phospho-S6 ribosomal protein (#4856; Cell Signaling Technology, Danvers, MA, USA; rabbit monoclonal, clone: 2F9, dilution: 1/400). After washing with PBS thrice, cells were incubated with the respective Alexa Fluor-labeled secondary antibodies (Molecular Probes/Thermo Fisher Scientific, Eugene, OR, USA; O/N, 4 °C; 1/200 dilution) diluted in Blocking One. Cells were finally stained with Hoechst 33342 (Thermo Fisher Scientific, Waltham, MA, USA; 2 µg mL^{-1} in PBS; O/N, 4 °C). After washing with PBS twice, cells were observed under a BZ-9000 or BZ-X810 fluorescence microscope (Keyence, Osaka, Japan). Acquired images were analyzed using CellProfiler[24] to obtain mean fluorescence intensity per cell.

Generation of 3D-PDAC Fibrotic Tissues: Methods for 3D-PDAC fibrotic tissue generation are as reported previously.[4,16] Cells after trypsinization were first incubated, upon gentle rocking, in Tris-buffered saline (pH 7.4) containing fibronectin (0.04 mg mL^{-1}; Sigma-Aldrich) and gelatin (0.04 mg mL^{-1}; Wako Pure Chemicals) for 30 min at RT. Cells were then briefly centrifuged, re-suspended in fresh culture media, and then seeded (1×10^6 insert^{-1}) on cell culture inserts with 0.4 µm pores (BD Falcon/Corning) for 24-well plates (BD Falcon/Corning), coated with fibronectin (0.12 mg mL^{-1}). This cell seeding density results in 3D-PDAC fibrotic tissues with a thickness of ≈15–20 µm, which is within the clinically observed range of the distance that an intravenously administered therapeutic agent must penetrate to reach a tumor target within the fibrotic human PDAC tumor microenvironment.[4] Transparent inserts were used for fluorescent staining and thickness measurements of 3D-PDAC fibrotic tissues, and translucent (high pore density) inserts for assessment of macromolecular permeability. Culture media were replaced every 24 h. Compounds were administered to 3D-PDAC fibrotic tissues beginning from 24 h after cell seeding at the time of medium change, except for the time course analyses of the duration of VU-6015929 treatment required to enhance macromolecular permeability where details are provided in the figure as a schematic (Figure S2A–C, Supporting Information).

For the generation of 3D-PDAC fibrotic tissues requiring knockdown, siRNA transfections were performed prior to 3D tissue generation. PSCs (6×10^5 cells) were first seeded onto 100 mm culture dishes (BD Falcon/Corning), and siRNAs were transfected 24 h post cell seeding as described above. Cells were harvested for generating 3D-PDAC fibrotic tissues 24 h after siRNA transfection.

Fluorescent Staining of 3D-PDAC Fibrotic Tissues: After 3 days of culture, 3D-PDAC fibrotic tissues were washed once with PBS and fixed with 4% (w/v) PFA/PBS (5 min, RT). After fixation, 3D-PDAC fibrotic tissues were blocked with Blocking One (1–2 h, RT) and then incubated with anti-collagen I antibody (ab138492; Abcam) diluted in Blocking One (1/1000 dilution; O/N, 4 °C). After washing with PBS thrice, 3D-PDAC fibrotic tissues were incubated with the respective Alexa Fluor-labelled secondary antibodies diluted in Blocking One (1/200 dilution; O/N, 4 °C). Finally, 3D-PDAC fibrotic tissues were stained with Hoechst 33342 (2 µg mL^{-1} in PBS; O/N, 4 °C). After washing with PBS thrice, culture insert membranes were carefully excised using a scalpel and mounted on coverslips using fluorescent mounting medium (Dako/Agilent, Santa Clara, CA, USA). Samples were then observed under a BZ-X810 fluorescence microscope. To visualize the collagen network within the 3D-PDAC fibrotic tissues, Z-stack images of 0.4 µm slices were obtained for maximum intensity projection of collagen staining using the BZ-H4A image analysis software (Keyence). For quantification of collagen I, insert-wide images were stitched using the BZ-H4A image analysis software and mean fluorescence intensity measured using ImageJ (NIH, Bethesda, MD, USA).

Thickness Measurements of 3D-PDAC Fibrotic Tissues: Measurement of the thickness of 3D-PDAC fibrotic tissues was performed as reported previously.[16] After 3 days of culture, 3D-PDAC fibrotic tissues were washed once with PBS, fixed with 4% (w/v) PFA/PBS (5 min, RT), and permeabilized with 0.2% (v/v) Triton X-100/PBS (20 min, RT). SYTOX Green nucleic acid stain (Molecular Probes/Thermo Fisher Scientific; 0.2 µM; O/N, 4 °C) was then used to stain cell nuclei. After washing with PBS thrice, culture insert membranes were carefully excised using a scalpel. Excised membranes were then mounted on coverslips using Dako fluorescent mounting medium. Samples were observed under a BZ-X810 fluorescence microscope, and Z-stack images of 0.5 µm slices were obtained. Images were 3D-reconstituted, and the thickness measured using the BZ-H4A image analysis software.

Assessment of the Macromolecular Permeability of 3D-PDAC Fibrotic Tissues: Macromolecular permeability of 3D-PDAC fibrotic tissues were assessed as reported previously.[16] 3 days after generating 3D-PDAC fibrotic tissues, culture media were replaced (0.45 mL inside the insert and 1 mL in the well). Afterward, 50 µL of the respective fluorescently labeled macromolecule (described below) to be assessed were gently loaded onto the inserts. The 3D-PDAC fibrotic tissues were incubated for another 24 h, after which the inserts were carefully removed and discarded. Media within the wells were collected and stored in the dark until measurement. Each sample (100 µL) was loaded onto clear 0.5 mL tubes (Greiner Bio-One, Kremsmünster, Austria) and measured using a fluorometer (DS-11 with

the FX module; DeNovix, Wilmington, DE, USA). The concentration of the macromolecule in the sample was determined from a standard curve obtained using known concentrations of the macromolecule diluted in culture media. The percentage of macromolecules that permeated the 3D tissues was calculated as $C/C_{\infty} \times 100$, where C is the measured sample concentration and C_{∞} is the theoretical concentration without 3D tissues at equilibrium. Given the volumes of culture media in the insert (total 0.5 mL) and the well (1 mL), C_{∞} equals $C_0/3$, where C_0 is the initial concentration of the macromolecule inside the insert.

The macromolecules used in this study are, as follows: FITC-labeled dextran (average molecular weight of 70, 150, or 2000 kDa; all from Sigma-Aldrich; 4 mg mL^{-1} in PBS), FITC-labeled bovine albumin (Sigma-Aldrich; 4 mg mL^{-1} in PBS), and FITC-labeled human IgG (Sigma-Aldrich; 4 mg mL^{-1} in PBS). The reported hydrodynamic radii of FITC-dextran (70, 150, and 2000 kDa), FITC-albumin, and FITC-IgG are ≈6, ≈8, ≈27, ≈3, and ≈5 nm, respectively.[53,54]

Assessment of Macromolecular Drug Delivery through 3D-PDAC Fibrotic Tissues: VU-6015929 was administered on day 1 and day 2 post 3D-PDAC fibrotic tissue generation. After pretreatment for 48 h, culture media containing VU-6015929 were replaced as follows: 0.5 mL media with either Doxil or Abraxane, both at 10 μg mL^{-1}, inside the insert and 1 mL media within the well. The 3D-PDAC fibrotic tissues were incubated for another 24 h, after which the inserts were carefully removed and discarded. Media within the wells were collected and used to treat MiaPaCa-2 cells seeded onto 6-well plates (1×10^5 $well^{-1}$) or 24-well plates (2×10^4 $well^{-1}$) for 48 h. Untreated MiaPaCa-2 cells as well as MiaPaCa-2 cells directly treated with Doxil or Abraxane at C_{∞} (i.e., 3.3 μg mL^{-1}) were included as negative and positive controls. MiaPaCa-2 cells were then fixed and stained with crystal violet as described above.

Reverse Transcription-Quantitative Polymerase Chain Reaction: PSCs (1×10^5 $well^{-1}$) were seeded onto 6-well plates. Transfection of siRNAs were performed 24 h after cell seeding as described above. Total RNA was isolated using the FastGene RNA Basic Kit (Nippon Genetics Co., Ltd., Tokyo, Japan) 48 h after siRNA transfection. Total RNA (1 μg) was reverse transcribed to complementary DNA (ReverTra Ace -α-; TOYOBO, Osaka, Japan) according to the manufacturer's protocol. Reverse transcription-quantitaive polymerase chain reaction (RT-qPCR) was performed using the THUNDERBIRD SYBR qPCR mix (TOYOBO) on the StepOne Plus real-time PCR system (Applied Biosystems, Foster City, CA, USA). Primer sequences are as follows (all primers obtained from Sigma Genosys): *ACTB* (Forward: 5′-TCACCCACACTGTGCCCATCTACGA-3′; Reverse: 5′-CAGCGGAACCGCTCATTGCCAATGG-3′), *COL1A1* (Forward: 5′- CCCTGGAAAGAATGGAGATG-3′; Reverse: 5′-CCATCCAAACCACTGAAACC-3′), *DDR1* (Forward: 5′- AGTGGAGATGCTGACATGAAGG-3′; Reverse: 5′-AAGCAGAGATGTCACTGTCTGG-3′), *DDR2* (Forward: 5′-TGGTGGCTGTGAAAATGCTC-3′; Reverse: 5′-TGATGTTTGGGTCCTTGAGC-3′), *ETV7* (Forward: 5′-AGACAAGGACGCCAAGATCTTC-3′; Reverse: 5′-TAGGTCATGTTCACCCGGTTC-3′), *GIT1* (Forward: 5′-TGATGTTAATGGCCGCACAC-3′; Reverse: 5′-ATTCTTGTGATCCGGCTTGC-3′), *MEAK7* (Forward: 5′-ACATGAAGCTGCAAGATGGC-3′; Reverse: 5′-AAGCCCTTGCAAATGACCAC-3′), *MTOR* (Forward: 5′-ATTGATACGCCCAGACCCTTG-3′; Reverse: 5′-TCTTGTTGGCTGCATTGTGC-3′), *RICTOR* (Forward: 5′-TGCTGTCACACTGCACATTC-3′; Reverse: 5′-AGGTTGCTTTGGTGGTGTTG-3′), and *RPTOR* (Forward: 5′- TGTGCCTGAATGTTGGTGTG-3′; Reverse: 5′-TTTGCACCGATGGTTTCCAG-3′). *ACTB* expression was used as the internal control for all RT-qPCR experiments.

Statistical Analysis: All statistical analyses were performed in GraphPad Prism 10 (GraphPad Software, Inc., La Jolla, CA, USA). In each graph, individual data points indicating biological replicates are shown as distinct points in the figure. Of note, graphs showing quantified fluorescence intensity are presented as SuperPlots,[25] color-coded to represent the intercellular variation observed in each experimental replicate. All quantitative data are presented as mean ± standard deviation (SD). The statistical tests performed are all two-sided, and details are provided in the respective figure legends. For all analyses, statistical significance was set a $p < 0.05$.

Supporting Information

Supporting Information is available from the Wiley Online Library or from the author.

Acknowledgements

This study was supported in part by Grant-in-Aid for Scientific Research (KAKENHI) from the Japan Society for the Promotion of Science (MY: JP24H00787, KO: JP21H03832 and JP21K19014, AM: JP23K24312, MRK: JP23H02653 and JP26293119, HYT: JP23K06279 and JP20K16989), Japan Science and Technology Agency (JST) through the open innovation platform for industry-academia co-creation (COI-NEXT) program (KO: JPMJPF2202), Okayama University (MRK and HYT), the Harmonic Ito Foundation (HYT), the Inamori Foundation (HYT), the Hokuto Foundation for Bioscience (HYT), the Research Foundation for Pharmaceutical Sciences (HYT), the Japan Foundation for Applied Enzymology (HYT), the Pancreas Research Foundation of Japan (HYT), the Sanyo Broadcasting Foundation (HYT), the Ryobi Teien Memory Foundation (HYT), and the KAWASAKI Foundation for Medical Science and Medical Welfare (HYT). The authors deeply thank Dr. Hiromi Matsubara (National Hospital Organization Okayama Medical Center) for the generous provision of experimental facilities. Further thanks to past and present members of the lab, especially Misaki Nakamura, Yu Seno, and Natsuki Kiriishi.

Conflict of Interest

The authors declare no conflict of interest.

Author Contributions

M.O. and M.K. contributed equally to this work. M.O.: conceptualization, formal analysis, investigation, writing-review & editing. M.K.: conceptualization, formal analysis, investigation, writing-review & editing. H.I.: formal analysis, investigation, writing-review & editing. H.O.-O.: methodology, software, writing-review & editing. H.T.: investigation, writing-review & editing. R.N.: investigation, writing-review & editing. T.N.: investigation, writing-review & editing. A.N.: methodology, writing-review & editing. M.Y.: funding acquisition, writing-review & editing. K.O.: funding acquisition, writing-review & editing. S.T.: resources, writing-review & editing. H.C.: conceptualization, writing-review & editing. A.M.: funding acquisition, resources, writing-review & editing. M.R.K.: conceptualization, funding acquisition, resources, supervision, writing-review & editing. H.Y.T.: conceptualization, data curation, formal analysis, funding acquisition, investigation, methodology, project administration, resources, software, supervision, validation, visualization, writing-original draft, writing-review & editing.

Data Availability Statement

The data that support the findings of this study are available from the corresponding author upon reasonable request.

Keywords

collagen, fibrosis, nanomedicine, pancreatic cancer, pancreatic stellate cell

Received: June 9, 2025
Revised: September 2, 2025
Published online:

[1] H. Y. Tanaka, T. Kurihara, T. Nakazawa, M. Matsusaki, A. Masamune, M. R. Kano, *Biomaterials* **2020**, *251*, 120077.
[2] H. Y. Tanaka, M. R. Kano, *Cancer Sci.* **2018**, *109*, 2085.
[3] H. Y. Tanaka, T. Nakazawa, A. Enomoto, A. Masamune, M. R. Kano, *Cancers* **2023**, *15*, 724.
[4] H. Y. Tanaka, K. Kitahara, N. Sasaki, N. Nakao, K. Sato, H. Narita, H. Shimoda, M. Matsusaki, H. Nishihara, A. Masamune, M. R. Kano, *Biomaterials* **2019**, *192*, 355.
[5] K. P. Olive, M. A. Jacobetz, C. J. Davidson, A. Gopinathan, D. McIntyre, D. Honess, B. Madhu, M. A. Goldgraben, M. E. Caldwell, D. Allard, K. K. Frese, G. DeNicola, C. Feig, C. Combs, S. P. Winter, H. Ireland-Zecchini, S. Reichelt, W. J. Howat, A. Chang, M. Dhara, L. Wang, F. Rückert, R. Grützmann, C. Pilarsky, K. Izeradjene, S. R. Hingorani, P. Huang, S. E. Davies, W. Plunkett, M. Egorin, et al., *Science* **2009**, *324*, 1457.
[6] P. Rawla, T. Sunkara, V. Gaduputi, *World J. Oncol.* **2019**, *10*, 10.
[7] A. J. Grossberg, L. C. Chu, C. R. Deig, E. K. Fishman, W. L. Hwang, A. Maitra, D. L. Marks, A. Mehta, N. Nabavizadeh, D. M. Simeone, C. D. Weekes, C. R. Thomas Jr, *Cancer J. Clin.* **2020**, *70*, 375.
[8] R. Ando, A. Sakai, T. Iida, K. Kataoka, Y. Mizutani, A. Enomoto, *Cancers* **2022**, *14*, 3315.
[9] M. Erkan, G. Adler, M. V. Apte, M. G. Bachem, M. Buchholz, S. Detlefsen, I. Esposito, H. Friess, T. M. Gress, H.-J. Habisch, R. F. Hwang, R. Jaster, J. Kleeff, G. Klöppel, C. Kordes, C. D. Logsdon, A. Masamune, C. W. Michalski, J. Oh, P. A. Phillips, M. Pinzani, C. Reiser-Erkan, H. Tsukamoto, J. Wilson, *Gut* **2012**, *61*, 172.
[10] M. B. Omary, A. Lugea, A. W. Lowe, S. J. Pandol, *J. Clin. Invest.* **2007**, *117*, 50.
[11] C. Tian, K. R. Clauser, D. Öhlund, S. Rickelt, Y. Huang, M. Gupta, D. R. Mani, S. A. Carr, D. A. Tuveson, R. O. Hynes, *Proc. Natl. Acad. Sci. USA* **2019**, *116*, 196098.
[12] L. Miao, C. M. Lin, L. Huang, *J. Controlled Release* **2015**, *219*, 192.
[13] B. Leitinger, *Int. Rev. Cell Mol. Biol.* **2014**, *310*, 39. .
[14] B. Leitinger, *Annu. Rev. Cell Dev. Biol.* **2011**, *27*, 265.
[15] S. Bansod, M. A. Saifi, C. Godugu, *Sci. Rep.* **2021**, *11*, 12894.
[16] H. Y. Tanaka, T. Nakazawa, T. Miyazaki, H. Cabral, A. Masamune, M. R. Kano, *J. Controlled Release* **2024**, *369*, 283.
[17] A. M. Waters, C. J. Der, *Perspect. Med.* **2018**, *8*, a031435.
[18] J. R. Infante, B. G. Somer, J. O. Park, C.-P. Li, M. E. Scheulen, S. M. Kasubhai, D.-Y. Oh, Y. Liu, S. Redhu, K. Steplewski, N. Le, A. randomised, *Eur. J. Cancer* **2014**, *50*, 2072.
[19] D. E. Jeffries, C. M. Borza, A. L. Blobaum, A. Pozzi, C. W. Lindsley, *ACS Med. Chem. Lett.* **2020**, *11*, 29.
[20] C. Jensen, Y. Teng, *Front. Mol. Biosci.* **2020**, *7*, 33.
[21] O. Lyass, A. Hubert, A. A. Gabizon, *Clin. Cancer Res.* **2001**, *7*, 3040.
[22] E. R. Gardner, W. L. Dahut, C. D. Scripture, J. Jones, J. B. Aragon-Ching, N. Desai, M. J. Hawkins, A. Sparreboom, W. D. Figg, *Clin. Cancer Res.* **2008**, *14*, 4200.
[23] C. M. Dawidczyk, C. Kim, J. H. Park, L. M. Russell, K. H. Lee, M. G. Pomper, P. C. Searson, *J. Controlled Release* **2014**, *187*, 133.
[24] D. R. Stirling, M. J. Swain-Bowden, A. M. Lucas, A. E. Carpenter, B. A. Cimini, A. Goodman, *BMC Bioinformatics* **2021**, *22*, 433.
[25] S. J. Lord, K. B. Velle, R. D. Mullins, L. K. Fritz-Laylin, *J. Cell Biol.* **2020**, *219*, 202001064.
[26] J. R. Infante, L. A. Fecher, G. S. Falchook, S. Nallapareddy, M. S. Gordon, C. Becerra, D. J. DeMarini, D. S. Cox, Y. Xu, S. R. Morris, V. G. Peddareddigari, N. T. Le, L. Hart, J. C. Bendell, G. Eckhardt, R. Kurzrock, K. Flaherty, H. A. Burris, W. A. Messersmith, *Lancet Oncol.* **2012**, *13*, 773.
[27] H.-G. Kim, L. Tan, E. L. Weisberg, F. Liu, P. Canning, H. G. Choi, S. A. Ezell, H. Wu, Z. Zhao, J. Wang, A. Mandinova, J. D. Griffin, A. N. Bullock, Q. Liu, S. W. Lee, N. S. Gray, *ACS Chem. Biol.* **2013**, *8*, 2145.
[28] W. R. Grither, G. D. Longmore, *Proc. Natl. Acad. Sci. USA* **2018**, *115*, E7786.
[29] H. Su, F. Yang, R. Fu, B. Trinh, N. Sun, J. Liu, A. Kumar, J. Baglieri, J. Siruno, M. Le, Y. Li, S. Dozier, A. Nair, A. Filliol, N. Sinchai, S. B. Rosenthal, J. Santini, C. M. Metallo, A. Molina, R. F. Schwabe, A. M. Lowy, D. Brenner, B. Sun, M. Karin, *Nature* **2022**, *610*, 366.
[30] S. Dagamajalu, D. A. B. Rex, G. P. Suchitha, A. B. Rai, S. Kumar, S. Joshi, R. Raju, T. S. K. Prasad, *J. Cell Commun. Signaling* **2023**, *17*, 1081.
[31] T. Tamura, T. Kodama, K. Sato, K. Murai, T. Yoshioka, M. Shigekawa, R. Yamada, H. Hikita, R. Sakamori, H. Akita, H. Eguchi, R. L. Johnson, H. Yokoi, M. Mukoyama, T. Tatsumi, T. Takehara, *J. Clin. Invest.* **2021**, *131*.
[32] G. Y. Liu, D. M. Sabatini, *Nat. Rev. Mol. Cell Biol.* **2020**, *21*, 183.
[33] H. Hirai, H. Sootome, Y. Nakatsuru, K. Miyama, S. Taguchi, K. Tsujioka, Y. Ueno, H. Hatch, P. K. Majumder, B.-S. Pan, H. Kotani, *Mol. Cancer Ther.* **2010**, *9*, 1956.
[34] C. M. Chresta, B. R. Davies, I. Hickson, T. Harding, S. Cosulich, S. E. Critchlow, J. P. Vincent, R. Ellston, D. Jones, P. Sini, D. James, Z. Howard, P. Dudley, G. Hughes, L. Smith, S. Maguire, M. Hummersone, K. Malagu, K. Menear, R. Jenkins, M. Jacobsen, G. C. M. Smith, S. Guichard, M. Pass, *Cancer Res.* **2010**, *70*, 288.
[35] F. C. Harwood, R. I. Klein Geltink, B. P. O'Hara, M. Cardone, L. Janke, D. Finkelstein, I. Entin, L. Paul, P. J. Houghton, G. C. Grosveld, *Sci. Adv.* **2018**, *4*, aar3938.
[36] J. T. Nguyen, F. S. Haidar, A. L. Fox, C. Ray, D. B. Mendonça, J. K. Kim, P. H. Krebsbach, *iScience* **2019**, *17*, 190.
[37] Z. He, P. J. Houghton, T. M. Williams, C. Shen, *Cell Cycle* **2021**, *20*, 742.
[38] L. J. Smithson, D. H. Gutmann, *Genes Dev.* **2016**, *30*, 1383.
[39] Y. Chen, S. Yang, J. Tavormina, D. Tampe, M. Zeisberg, H. Wang, K. K. Mahadevan, C.-J. Wu, H. Sugimoto, C.-C. Chang, R. R. Jenq, K. M. McAndrews, R. Kalluri, *Cancer Cell* **2022**, *40*, 818.
[40] J. P. R. O. Orgel, R. S. Madhurapantula, *Biochim. Biophys. Acta, Mol. Cell. Res.* **2019**, *1866*, 118478.
[41] J. M. Ruggeri, J. Franco-Barraza, A. Sohail, Y. Zhang, D. Long, M. Pasca di Magliano, E. Cukierman, R. Fridman, H. C. Crawford, *Am. J. Pathol.* **2020**, *190*, 1735.
[42] S. Moll, A. Desmoulière, M. J. Moeller, J.-C. Pache, L. Badi, F. Arcadu, H. Richter, A. Satz, S. Uhles, A. Cavalli, F. Drawnel, L. Scapozza, M. Prunotto, *Biochim. Biophys. Acta, Mol. Cell. Res.* **2019**, *1866*, 118474.
[43] M. Platé, D. Guillotin, R. C. Chambers, *Eur. Respir. Rev.* **2020**, *29*, 200269.
[44] B. Garg, B. Giri, S. Modi, V. Sethi, I. Castro, O. Umland, Y. Ban, S. Lavania, R. Dawra, S. Banerjee, S. Vickers, N. B. Merchant, S. X. Chen, E. Gilboa, S. Ramakrishnan, A. Saluja, V. Dudeja, *Gastroenterology* **2018**, *155*, 880.
[45] N. Wu, X.-F. Xu, J.-Q. Xin, J.-W. Fan, Y.-Y. Wei, Q.-X. Peng, L.-F. Duan, W. Wang, H. Zhang, *J. Cell. Mol. Med.* **2021**, *25*, 2213.
[46] A. Rajadurai, H. Tsao, *JID Innovation* **2023**, *4*, 100248.
[47] E. Kun, Y. T. M. Tsang, C. W. Ng, D. M. Gershenson, K. K. Wong, *Cancer Treat. Rev.* **2021**, *92*, 102137.
[48] M. H. Jenkins, W. Croteau, D. W. Mullins, C. E. Brinckerhoff, *Matrix Biol.* **2015**, *PLX4032*, 66.
[49] H. E. Brighton, S. P. Angus, T. Bo, J. Roques, A. C. Tagliatela, D. B. Darr, K. Karagoz, N. Sciaky, M. L. Gatza, N. E. Sharpless, G. L. Johnson, J. E. Bear, *Cancer Res.* **2018**, *78*, 542.
[50] J. Prakash, Y. Shaked, *Cancer Discovery* **2024**, *14*, 1375.

[51] N. Reunanen, M. Foschi, J. Han, V. M. Kahari, *J. Biol. Chem.* **2000**, *275*, 346349.
[52] S. Hamada, A. Masamune, T. Takikawa, N. Suzuki, K. Kikuta, M. Hirota, H. Hamada, M. Kobune, K. Satoh, T. Shimosegawa, *Biochem. Biophys. Res. Commun.* **2012**, *421*, 349.
[53] J. Ambati, C. S. Canakis, J. W. Miller, E. S. Gragoudas, A. Edwards, D. J. Weissgold, I. Kim, F. C. Delori, A. P. Adamis, *Invest. Ophthalmol. Visual Sci.* **2000**, *41*, 1181.
[54] L. Lebrun, G.-A. Junter, *J. Membr. Sci.* **1994**, *88*, 253.